

Implementing magnetic properties on demand with a dynamic Lanthanoid-Organic Framework

Iván Gómez-Muñoz,^{a†} Ziqi Hu,^{a†} Iñigo J. Vitórica-Yrezábal,^b Eugenio Coronado,^a and Guillermo Mínguez Espallargas^{*a}

^aInstituto de Ciencia Molecular (ICMol), Universidad de Valencia, c/ Catedrático José Beltrán 2, Paterna, 46980, Spain.

^bDepartamento de Química Inorgánica, Facultad de Ciencias, Universidad de Granada. Av. Fuente Nueva, 18070, Granada, Spain.

† These authors contributed equally

Summary

S1. Experimental details	2
S2. ICP-MS	3
S3. Single-crystal X-ray diffraction.....	3
S4. Powder X-ray diffraction	12
S5. Stability studies	14
S6. Thermogravimetric analysis	4
S7. ^1H NMR spectroscopy	6
S8. Gas sorption measurements	9
S9. AC and DC magnetic measurements	11
S10. Qubit properties.....	23
References.....	33

S1. Experimental details

LOFs synthesis

The synthesis consists of a modified method reported in the literature¹. All reactants were commercially available and used without further purification.

Synthesis of Ln-LOFs. $\text{LnCl}_3 \cdot x\text{H}_2\text{O}$ (where $\text{Ln} = \text{La, Ce, Pr, Sm, Eu, Gd, Tb, Dy, Ho, Er, Lu, and Y}$) (0.09 g, 0.25 mmol) (Sigma-aldrich) and 1,3,5-tri(4-carboxyphenyl)benzene (H_3BTB) (0.11 g, 0.25 mmol) (Alfa-Aesar) were dissolved in DMF (5 mL). The resulting solution was transferred to a 15 mL glass vial and heated at 120 °C for 72 h in an oven. After cooling to room temperature, the crystals were filtrated under vacuum and washed with ethanol, letting them dry under air. Anal. Calc. $\text{La}(\text{C27H15O}_6) \cdot 1.62\text{DMF}$ (692.73): C, 55.24; H, 3.83; N, 3.28 %. Found: C, 52.40; H, 3.98; N, 3.77 %. $\text{Ce}(\text{C27H15O}_6) \cdot 1.63\text{DMF}$ (694.672): C, 55.14; H, 3.83; N, 3.29 %. Found: C, 52.10; H, 3.86; N, 3.52 %. $\text{Pr}(\text{C27H15O}_6) \cdot 1.75\text{DMF}$ (704.235): C, 55.00; H, 3.90; N, 3.48 %. Found: C, 51.81; H, 3.94; N, 3.60 %. $\text{Dy}(\text{C27H15O}_6) \cdot 3\text{DMF}$ (817.196): C, 52.91; H, 4.44; N, 5.14 %. Found: C, 50.44; H, 4.35; N, 4.62 %.

Synthesis of Ln-LOF1_des. Crystals of Ln-LOF1 were heated at 150 °C under vacuum for 3 hours. Anal. Calc. $\text{La}(\text{C27H15O}_6) \cdot 0.62\text{DMF}$ (619.635): C, 55.94; H, 3.15; N, 1.4 %. Found: C, 52.88; H, 3.16; N, 1.10 %.

Synthesis of Ln-LOF1_act. Crystals of Ln-LOF1 were heated at 300 °C under vacuum for 3 hours. Anal. Calc. $\text{La}(\text{C27H15O}_6)$ (574.317): C, 56.47; H, 2.63; N, 0.00%. Found: C, 55.28; H, 2.69; N, 0.09 %.

Synthesis of La-Dy-LOF1 20%. $\text{LaCl}_3 \cdot 7\text{H}_2\text{O}$ (0.09 g, 0.25 mmol) (Sigma-aldrich), $\text{DyCl}_3 \cdot 6\text{H}_2\text{O}$ (0.02 g, 0.05 mmol) and H_3BTB (0.11 g, 0.25 mmol) (Alfa-Aesar) were dissolved in DMF (5 mL). The resulting solution was transferred to a 15 mL glass vial and heated at 120 °C for 72 h in an oven. After cooling to room temperature, the crystals were filtered and washed with ethanol.

Synthesis of La-Gd-LOF1 0.1%. $\text{LaCl}_3 \cdot 7\text{H}_2\text{O}$ (0.09 g, 0.25 mmol) (Sigma-aldrich), $\text{GdCl}_3 \cdot 6\text{H}_2\text{O}$ (0.1 mL of a 1mg/mL solution, 0.25 µmol/ml) and H_3BTB (0.11 g, 0.25 mmol)

(Alfa-Aesar) were dissolved in DMF (5 mL). The resulting solution was transferred to a 15 mL glass vial and heated to 120 °C for 72 h in an oven. After cooling to room temperature, the crystals were filtered and washed with ethanol.

S2. ICP-MS

Table S1. Inductively coupled plasma spectroscopy results for La-Dy-LOF1 (20%) and La-Gd-LOF1 (20%). Two measurements on two different batches of the materials have been performed.

Compound	La (mmol/g)	Dy (mmol/g)	Gd (mmol/g)	% Dy	% Gd
La-Dy-LOF1 (1)	0.667	0.161	–	19.5	–
La-Dy-LOF1 (2)	0.531	0.146	–	21.6	–
La-Gd-LOF1 (1)	1.123	–	1.2×10^4	–	0.10
La-Gd-LOF1 (2)	1.008	–	1.2×10^4	–	0.12

S3. Single-crystal X-ray diffraction

X-ray Diffraction: Single crystal X-ray diffraction studies were performed on a Rigaku XtaLAB Synergy S diffractometer (Cu) X-ray source ($\lambda = 1.54184 \text{ \AA}$) (for **La-LOF1_des** structure) and a Rigaku Oxford Diffraction Supernova diffractometer (Mo) X-ray source ($\lambda = 0.71073 \text{ \AA}$) for the rest of structures, equipped with an HyPix-6000HE and an EOS CCD detectors respectively. The temperature during data collection was controlled by means of a dry N₂(g) cryostream (Oxford Cryostream 800). Suitable single crystals were selected and mounted on loops. CrysAlisPro software was used to collect and reduce the data. Adsorption corrections were applied using empirical methods using symmetry equivalent reflections combined with measurements at different azimuthal angles implemented using SCALE3 ABSPACK. The structure was initially solved using the SHELXT² program using an intrinsic phasing method

implemented through OLEX2³ (v1.5), and refined using SHELXL⁴ least squares refinement procedures against all F^2 values. All non-hydrogen atoms were refined anisotropically, or isotropically when this was not possible. Hydrogen atoms were placed in calculated positions and refined with idealised geometries and assigned fixed occupancies and isotropic displacement parameters. DMF molecules in as-synthetized and desolvated forms were located after completion of the framework structure by inspection of residual electron density. DMF molecules were modelled by fitting a rigid body model to electron density resembling DMF. When possible, the guest molecules were modelled anisotropically, and their occupancies refined against a single free variable. Disordered ligand positions were refined against the same free variable with a total occupancy over both positions fixed to a value of 1. Data for **Ce-LOF1_as** and **Ce-LOF1_des** crystals presented resolutions of 0.9 and 1.0 Å, so the data was trimmed accordingly. In general, crystal structures presented large regions of electron density close to the lanthanoid metal centres. This phenomenon is well known in lanthanoids, and it could be attributed to the X-ray absorption. Crystal face indexing or spherical absorption correction was attempted to account with the X-ray absorption, unsuccessfully. Crystals of **Dy-LOF2** were twinned and the data was processed as a two-component twin. Solvent mask protocol implemented in OLEX2 was used to account with the residual electron density in **La-LOF1_reDMF**, obtaining a DMF molecule per formula unit. Crystallographic information files CCDC 2384447-2384455 contain full details for all crystal structures reported.

Table S2. Crystallographic information of compounds **La-LOF1_as**, **La-LOF1_des**, **La-LOF1_act**, and **La-LOF1_reDMF**.

Identification code	LaLOF1_as	LaLOF1_des	LaLOF1_act	LaLOF1_reDMF
Empirical formula	C _{33.3} H _{29.7} LaN _{2.1} O _{8.1}	C _{28.3} H _{21.5} LaN _{0.4} O _{8.2}	C ₂₇ H _{15.8} LaO _{6.4}	C _{35.3} H _{34.3} LaN _{2.8} O _{8.8}
Formula weight	727.80	637.17	581.51	775.44
Temperature/K	120(2)	120(2)	120(2)	120(2)
Crystal system	monoclinic	monoclinic	monoclinic	monoclinic
Space group	<i>P</i> 2 ₁ / <i>c</i>	<i>P</i> 2 ₁ / <i>n</i>	<i>P</i> 2 ₁ / <i>c</i>	<i>P</i> 2 ₁ / <i>c</i>
<i>a</i> /Å	15.0013(6)	15.4232(6)	12.1008(4)	16.7495(3)
<i>b</i> /Å	27.7449(9)	20.5544(9)	27.7464(8)	26.5927(6)
<i>c</i> /Å	16.1774(9)	32.2850(11)	7.8237(2)	8.4965(2)
$\alpha/^\circ$	90	90	90	90
$\beta/^\circ$	97.287(4)	94.546(4)	93.673(3)	95.014(2)
$\gamma/^\circ$	90	90	90	90
Volume/Å ³	6678.8(5)	10202.6(7)	2621.44(13)	3769.98(14)
Z	8	16	4	4
$\rho_{\text{calc}}/\text{g/cm}^3$	1.448	1.659	1.473	1.366
μ/mm^{-1}	1.330	13.395	1.659	1.185
F(000)	2928.0	5066.0	1144.0	1568.0
Crystal size/mm ³	0.12 × 0.02 × 0.02	0.07 × 0.053 × 0.02	0.18 × 0.05 × 0.02	0.08 × 0.04 × 0.02
Radiation	Mo K _α ($\lambda = 0.71073$)	Cu K _α ($\lambda = 1.54184$)	Mo K _α ($\lambda = 0.71073$)	Mo K _α ($\lambda = 0.71073$)
2Θ range for data collection/°	5.62 to 50.248 -17 ≤ <i>h</i> ≤ 17 -32 ≤ <i>k</i> ≤ 32 -19 ≤ <i>l</i> ≤ 19	5.102 to 137.48 -18 ≤ <i>h</i> ≤ 13 -24 ≤ <i>k</i> ≤ 23 -38 ≤ <i>l</i> ≤ 38	5.988 to 52.886 -15 ≤ <i>h</i> ≤ 14 -34 ≤ <i>k</i> ≤ 33 -9 ≤ <i>l</i> ≤ 9	5.706 to 52.742 -20 ≤ <i>h</i> ≤ 20 -33 ≤ <i>k</i> ≤ 31 -10 ≤ <i>l</i> ≤ 10
Index ranges				
Reflections collected	20073 20073	70344 18640	7879 7879	68979 7663
Independent reflections	[R _{int} = 0.125 R _{sigma} = 0.1741]	[R _{int} = 0.0809 R _{sigma} = 0.0593]	[R _{int} = 0.117 R _{sigma} = 0.1437]	[R _{int} = 0.1304 R _{sigma} = 0.0989]
Data/restraints/parameters	20073/685/727	18640/303/1381	7879/484/290	7663/197/392
Goodness-of-fit on F ²	0.978	1.216	1.122	1.047
Final R indexes [I>=2σ (I)]	R ₁ = 0.0807 wR ₂ = 0.2073	R ₁ = 0.1061 wR ₂ = 0.2785	R ₁ = 0.0956 wR ₂ = 0.2867	R ₁ = 0.0811 wR ₂ = 0.1908
Final R indexes [all data]	R ₁ = 0.1347 wR ₂ = 0.2310	R ₁ = 0.1360 wR ₂ = 0.3143	R ₁ = 0.1508 wR ₂ = 0.3031	R ₁ = 0.1155 wR ₂ = 0.2083
Largest diff. peak/hole / e Å ⁻³	3.75/-1.91	7.25/-2.29	3.56/-5.34	3.03/-2.02

Table S3. Crystallographic information of compounds **Ce-LOF1_as**, **Ce-LOF1_des**, and **Ce-LOF1_act**.

Identification code	Ce-LOF1_as	Ce-LOF1_des	Ce-LOF1_act
Empirical formula	$C_{32.55}H_{27.95}CeN_{1.85}O_{7.85}$	$C_{28.5}H_{19}CeN_{0.5}O_{6.75}$	$C_{27}H_{15}CeO_6$
Formula weight	710.74	616.56	575.51
Temperature/K	120(2)	120(2)	120(2)
Crystal system	monoclinic	monoclinic	monoclinic
Space group	$P2_1/c$	$P2_1/n$	$P2_1/c$
$a/\text{\AA}$	15.0927(3)	15.3286(3)	12.1955(7)
$b/\text{\AA}$	27.9263(5)	20.5857(4)	27.6141(12)
$c/\text{\AA}$	16.1650(3)	32.2184(4)	7.7042(4)
$\alpha/^\circ$	90	90	90
$\beta/^\circ$	97.249(2)	94.4230(10)	93.382(4)
$\gamma/^\circ$	90	90	90
Volume/ \AA^3	6758.8(2)	10136.2(3)	2590.0(2)
Z	8	16	4
$\rho_{\text{calc}}/\text{g/cm}^3$	1.397	1.616	1.476
μ/mm^{-1}	1.395	1.842	1.794
F(000)	2856.0	4888.0	1132.0
Crystal size/mm ³	$0.08 \times 0.02 \times 0.01$	$0.17 \times 0.08 \times 0.02$	$0.18 \times 0.08 \times 0.02$
Radiation	Mo K _α ($\lambda = 0.71073$)	Mo K _α ($\lambda = 0.71073$)	Mo K _α ($\lambda = 0.71073$)
2θ range for data collection/°	5.592 to 46.512	5.686 to 41.624	5.902 to 52.74
Index ranges	-16 ≤ h ≤ 16 -31 ≤ k ≤ 31 -17 ≤ l ≤ 17	-15 ≤ h ≤ 15 -20 ≤ k ≤ 20 -32 ≤ l ≤ 32	-15 ≤ h ≤ 14 -21 ≤ k ≤ 34 -8 ≤ l ≤ 9
Reflections collected	114197 9681	221389 10599	10581 5004
Independent reflections	[$R_{\text{int}} = 0.1565$ $R_{\text{sigma}} = 0.0808$]	[$R_{\text{int}} = 0.1634$ $R_{\text{sigma}} = 0.0652$]	[$R_{\text{int}} = 0.0869$ $R_{\text{sigma}} = 0.1726$]
Data/restraints/parameters	9681/678/885	10599/1235/1321	5004/336/307
Goodness-of-fit on F^2	1.046	1.022	1.032
Final R indexes [$I \geq 2\sigma(I)$]	$R_1 = 0.0470$ $wR_2 = 0.1102$	$R_1 = 0.0795$ $wR_2 = 0.1942$	$R_1 = 0.0745$ $wR_2 = 0.1236$
Final R indexes [all data]	$R_1 = 0.0734$ $wR_2 = 0.1214$	$R_1 = 0.1181$ $wR_2 = 0.2288$	$R_1 = 0.1586$ $wR_2 = 0.1610$
Largest diff. peak/hole / e \AA^{-3}	1.62/-0.91	4.17/-2.25	2.41/-1.88

Table S4. Crystallographic information of compounds **Pr-LOF1_as**, and **Dy-LOF1_as**.

Identification code	Pr-LOF1_as	Dy-LOF1_as
Empirical formula	C _{31.5} H _{27.5} N _{1.5} O _{8.5} Pr	C ₃₆ H ₃₇ DyN ₃ O _{9.5}
Formula weight	703.96	826.18
Temperature/K	120(2)	120(2)
Crystal system	monoclinic	monoclinic
Space group	P2 ₁ /c	P2 ₁
<i>a</i> /Å	15.0438(3)	8.0212(5)
<i>b</i> /Å	28.0476(6)	26.890(2)
<i>c</i> /Å	16.0831(4)	16.3817(18)
$\alpha/^\circ$	90	90
$\beta/^\circ$	97.259(2)	92.297(8)
$\gamma/^\circ$	90	90
Volume/Å ³	6731.8(3)	3530.5(5)
Z	8	4
ρ_{calc} g/cm ³	1.389	1.554
μ/mm^{-1}	1.496	2.176
F(000)	2832.0	1664.0
Crystal size/mm ³	0.12 × 0.04 × 0.03	0.03 × 0.03 × 0.02
Radiation	Mo K _α ($\lambda = 0.71073$)	Mo K _α ($\lambda = 0.71073$)
2Θ range for data collection/°	5.65 to 55.87	5.748 to 52.884
Index ranges	-19 ≤ <i>h</i> ≤ 17 -36 ≤ <i>k</i> ≤ 23 -19 ≤ <i>l</i> ≤ 20	-9 ≤ <i>h</i> ≤ 10 -33 ≤ <i>k</i> ≤ 33 -19 ≤ <i>l</i> ≤ 19
Reflections collected	28894	12355
Independent reflections	13509	12355
Data/restraints/parameters	[R _{int} = 0.0513 R _{sigma} = 0.0968]	[R _{int} = 0.1312 R _{sigma} = 0.1774]
Goodness-of-fit on F ²	1.052	0.790
Final R indexes [I>=2σ (I)]	R ₁ = 0.0503, wR ₂ = 0.1059	R ₁ = 0.0505, wR ₂ = 0.0734
Final R indexes [all data]	R ₁ = 0.0755, wR ₂ = 0.1209	R ₁ = 0.0735, wR ₂ = 0.0785
Largest diff. peak/hole / e Å ⁻³	1.86/-1.16	1.49/-0.95
Flack parameter		0.425(13)

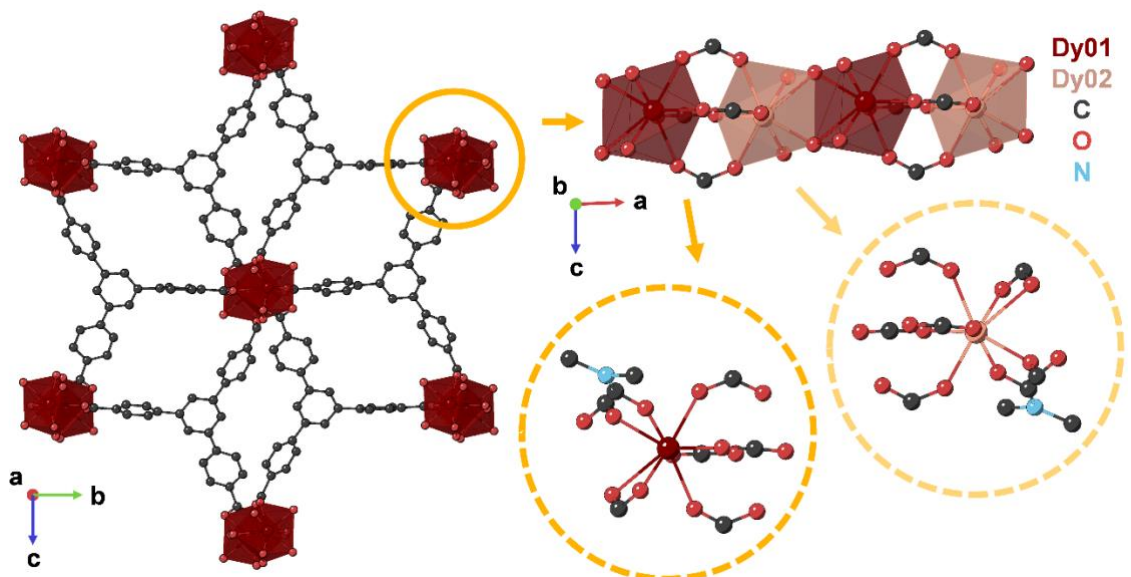


Figure S1. (Left) Scheme of LOF2 [$\text{Ln}(\text{BTB})\cdot 3\text{DMF}$] structure. Hydrogen atoms and solvent molecules have been omitted for clarity. (Top right) Rodlike chains of two crystallographically different lanthanoid atoms are depicted in dark and light red. (Bottom right) Coordination environment of the lanthanoid centres.

The LOF2 structure comprises two crystallographically independent lanthanoid atoms, which are linked to eight oxygens. Four of these oxygens are chelating carboxylates from the BTB ligands, three are from carboxylates shared with the neighboring lanthanoid, and the last one comes from a DMF molecule.

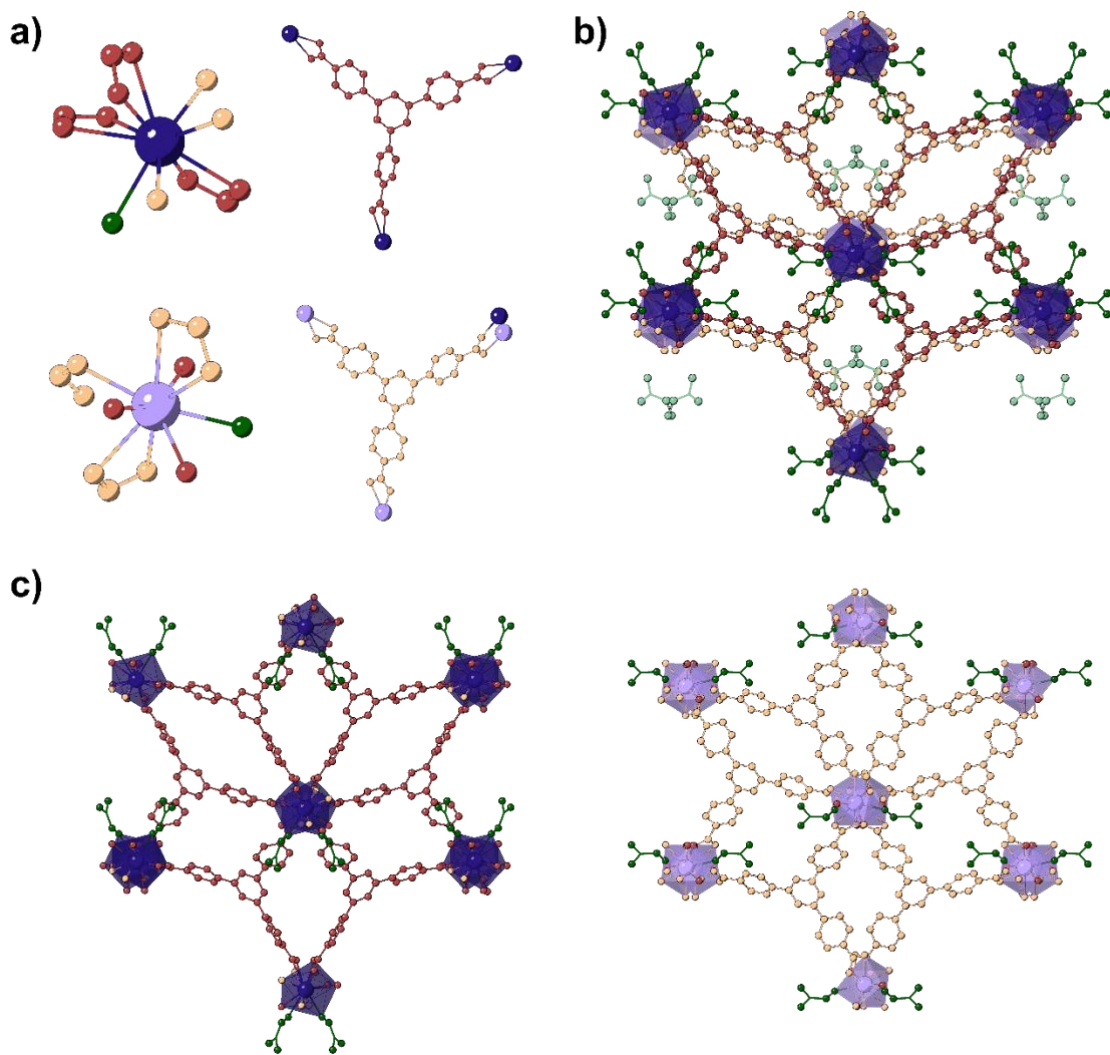


Figure S2. a) Schematic representation and coordination environment of La01 (dark blue), BTB01 (red), La02 (violet), and BTB02 (beige). b) **La-LOF1_as** structure where the DMF molecules are depicted in dark green (coordinated) and light green (solvated). c) Scheme of the two segregated frameworks that comprise **La-LOF1_as** structure.

For LOF1, each BTB ligand is coordinated to three different chains through its carboxylates. Within the chains, the La atoms are linked to each other by oxo-groups, alternating between the two crystallographically independent La's (La01 and La02). Each La interacts primarily with its corresponding BTB ligand (BTB01 or BTB02), resulting in a segregated structure (Figure S2 and Figure S3). In this way, La01 is linked to three different BTB01 ligands through both oxygens of their carboxylate groups, three additional single oxygens coming from three BTB02, and one

DMF molecule, obtaining a total coordination number of 10. However, the case for La02 differs slightly. This is because the bond with one of the three BTB02 ligands occurs through only one oxygen of the carboxylate, resulting in a total coordination number of 9 (Figure S2a). In this structure, it is possible to distinguish between two types of DMF molecules, the ones coordinated with the La ions and the ones located within the pores of the MOF.

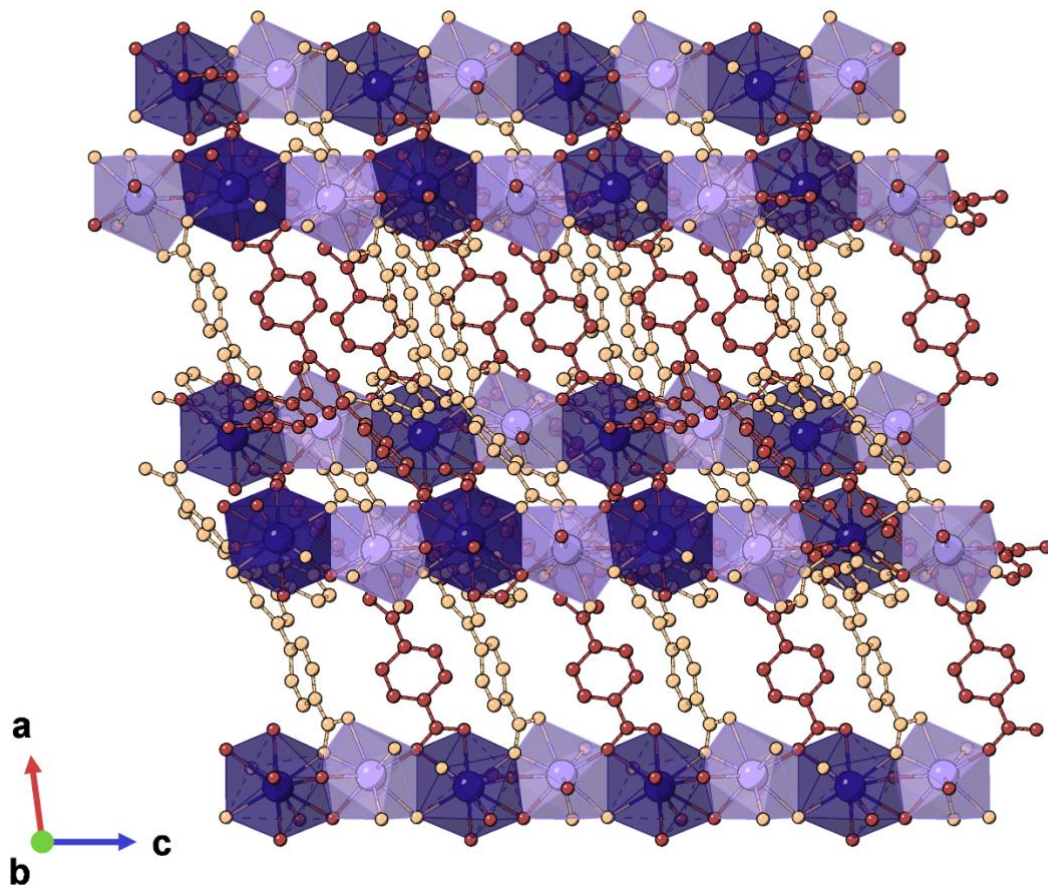


Figure S3. Side view along the *b*-axis of **La-LOF1_as** structure.

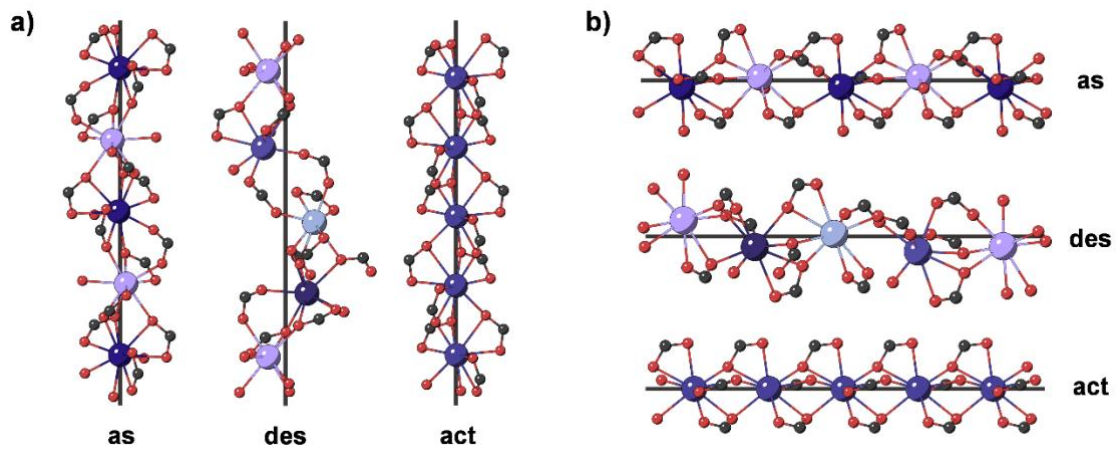


Figure S4. Alignment of La's atoms in the three different La-LOF1 phases. (a) Top view. (b) Side view. Crystallographically independent La atoms are depicted in different colors in each form.

S4. Powder X-ray diffraction

Powder X-Ray Diffraction (**PXRD**) experiments were acquired on an X-ray diffractometer (PANalytical Empyrean) with copper as a radiation source (Cu K_α , 1.5418 \AA) on as-synthesized samples, on desolvated samples (heated at 150°C under vacuum for 5 hours) and on activated samples (heated at 300°C under vacuum for 5 hours) (Figure S5). The thermal study (Figure 2c) was performed by measuring the pattern after continuously heating the sample under vacuum at $50, 60, 75, 100, 150, 200, 225$, and 300°C . The derivatives of other lanthanoids (Sm, Eu, Gd, Tb, Dy, Ho, Er, Lu, and Y) were also synthesized, but the resulting framework was found to be rigid (Figure S6). The reason for this is typically attributed to the lanthanoid contraction phenomenon. Smaller lanthanoids form weaker Ln–O bonds, which are more likely to induce flexibility in the structure⁵.

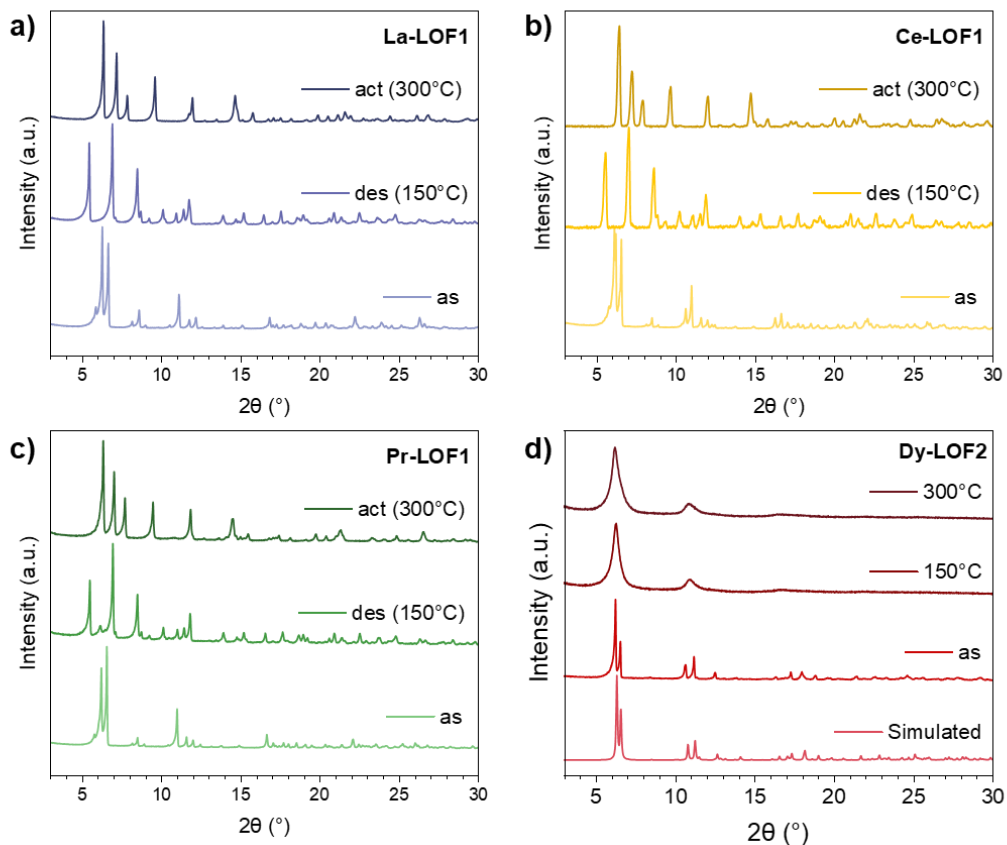


Figure S5. PXRD patterns for La-LOF1 (a), Ce-LOF1 (b), Pr-LOF1 (c), and Dy-LOF2 (d).

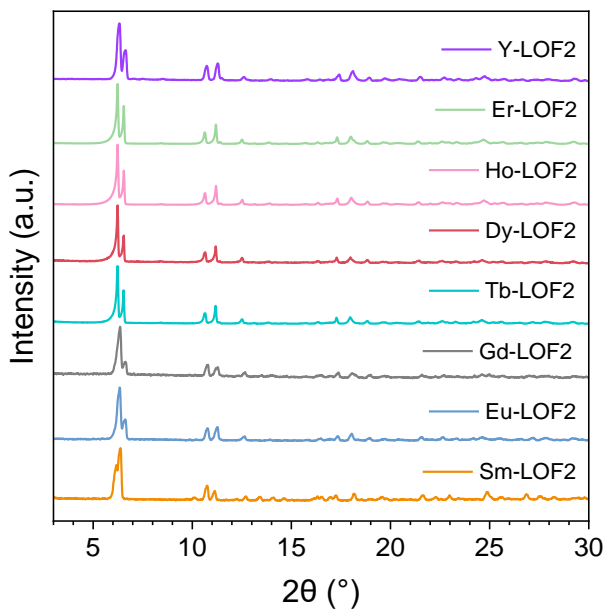


Figure S6. PXRD patterns for the rigid LOFs.

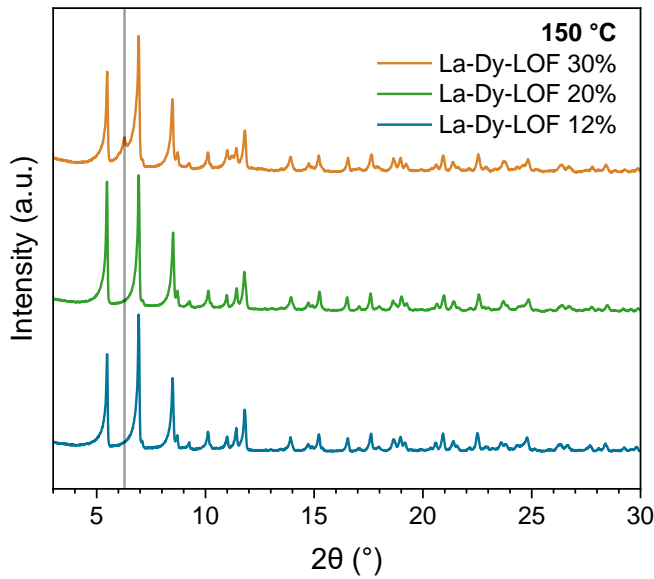


Figure S7. PXRD patterns of hybrid La-Dy-LOF1 with different Dy-content. The materials were heated at 150 °C in order to confirm the dynamic behavior of the original La-LOF1 matrix. The appearance of a peak at 6.27° (indicated with a grey line) in La-Dy-LOF1 30% shows the separate formation of Dy-LOF2 rigid structure.

S5. Stability studies

The crystals of La-LOF1_as, **des**, and **act** forms were soaked in different solvents at room temperature for 3 hours and later filtered.

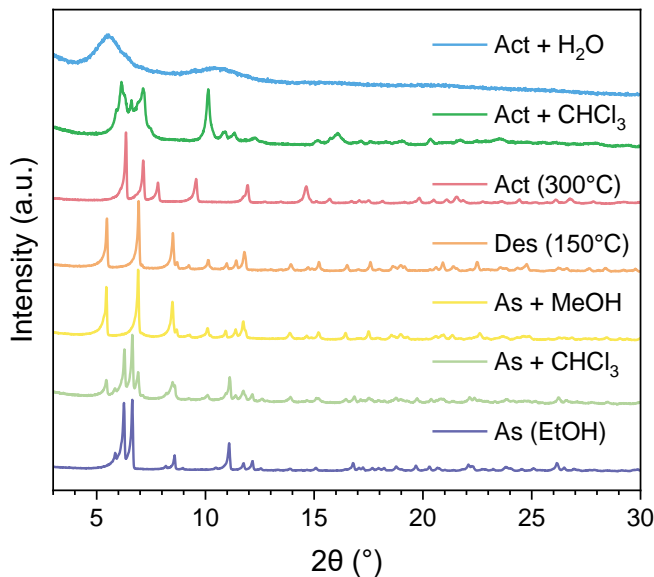


Figure S8. PXRD patterns of the different phases of La-LOF1 after being immersed in different solvents.

A general solvent interaction study revealed that **La-LOF1_as** slightly transits to **La-LOF1_des** after being immersed in chloroform while methanol leads to a full conversion of the structure (Figure S8). This indicates that the DMF molecules within the pores are displaced by the solvent. On the other hand, the immersion of **La-LOF1_act** in different solvents does not provide any recovery of the previous phases.

Reversibility study. Re-immersion in DMF

An open vial with few crystals of **La-LOF1_des** and **act** was placed in a beaker with a small amount of DMF inside. The beaker was left at room temperature covered with a watch glass overnight.

The reversibility of the different phase transitions of La-LOF1 was studied. Whereas **La-LOF1_des** crystals transited back to **La-LOF1_as** form, crystals of **La-LOF1_act** originated a brand new phase (**La-LOF1_reDMF**). Moreover, the reactivation of this new phase does not provide the original **La-LOF1_act** form but leads to the formation of another new phase instead (**La-LOF1_reAct**). The crystallinity of this last phase is lower than the previous phases, probably due to the long treatment the sample has been exposed to. In this case, heating **La-LOF1_reDMF** at 150 °C or 300 °C does not suggest any other phase transition, since the only observable difference in both diffractograms is a small loss of crystallinity. However, the reversibility between **La-LOF1_reDMF** and **La-LOF1_reAct** was confirmed by performing several cycles of heating and DMF-exposure.

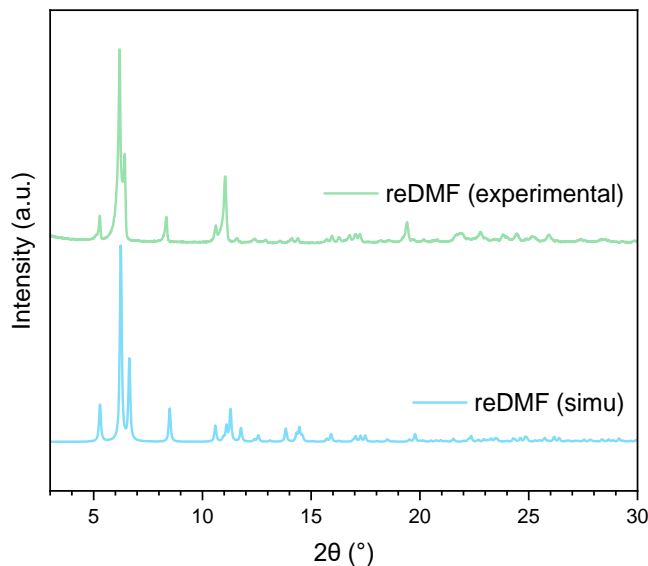


Figure S9. Simulated PXRD of **La-LOF1_reDMF** (blue) compared to the experimental one (green).

Table S5. Pawley refinements were performed using TOPAS 6.0.

	a (Å)	b (Å)	c (Å)	β (°)
La-LOF1_as (SCXRD)	15.0013(6)	27.7449(9)	16.1774(9)	97.287(4)
La-LOF1_as	15.058(3)	27.980(2)	16.300(3)	96.59(2)
La-LOF1_des (SCXRD)	15.4232(6)	20.5544(9)	32.2850(11)	94.546(4)
La-LOF1_des	15.526(8)	20.632(2)	32.107(6)	94.49(3)
La-LOF1_act (SCXRD)	12.1008(4)	27.7464(8)	7.8237(2)	93.673(3)
La-LOF1_act	12.3066(12)	27.654(3)	7.8120(19)	92.926(16)
La-LOF1_reDMF (SCXRD)	16.7495(3)	26.5927(6)	8.4965(2)	95.014(2)
La-LOF1_reDMF	16.602(9)	27.310(14)	8.352(4)	95.21(6)
Ce-LOF1_as (SCXRD)	15.0927(3)	27.9263(5)	16.1650(3)	97.249(2)
Ce-LOF1_as	14.968(3)	28.049(5)	16.043(3)	97.91(3)
Ce-LOF1_des (SCXRD)	15.3286(3)	20.5857(4)	32.2184(4)	94.4230(10)
Ce-LOF1_des	15.506(14)	20.590(3)	32.068(10)	93.96(5)
Ce-LOF1_act (SCXRD)	12.1955(7)	27.6141(12)	7.7042(4)	93.382(4)
Ce-LOF1_act	12.3059(17)	27.712(4)	7.7189(19)	92.988(18)
Pr-LOF1_as (SCXRD)	15.0438(3)	28.0476(6)	16.0831(4)	97.259(2)
Pr-LOF1_as	15.302(2)	28.285(3)	16.254(7)	96.43(4)
La-LOF1_des (SCXRD)	15.4232(6)	20.5544(9)	32.2850(11)	94.546(4)
Pr-LOF1_des	15.416(6)	20.679(3)	31.997(8)	93.92(4)
La-LOF1_act (SCXRD)	12.1008(4)	27.7464(8)	7.8237(2)	93.673(3)
Pr-LOF1_act	12.528(2)	27.737(5)	7.733(3)	93.24(4)
Dy-LOF2 (SCXRD)	8.0212(5)	26.890(2)	16.3817(18)	92.297(8)
Sm-LOF2	8.169(5)	26.945(12)	16.200(6)	90.71(7)
Eu-LOF2	7.968(6)	26.975(5)	16.5138(19)	90.93(5)
Gd-LOF2	7.940(7)	26.927(9)	16.527(3)	91.51(8)
Tb-LOF2	7.908(2)	26.880(3)	16.5536(14)	92.20(3)
Dy-LOF2	7.891(2)	26.848(3)	16.5430(14)	92.15(4)
Ho-LOF2	7.8850(18)	26.825(3)	16.5600(15)	92.23(2)
Er-LOF2	7.8721(19)	26.807(3)	16.545(13)	91.98(3)
Y-LOF2	7.995(4)	26.845(4)	16.5624(19)	92.50(2)

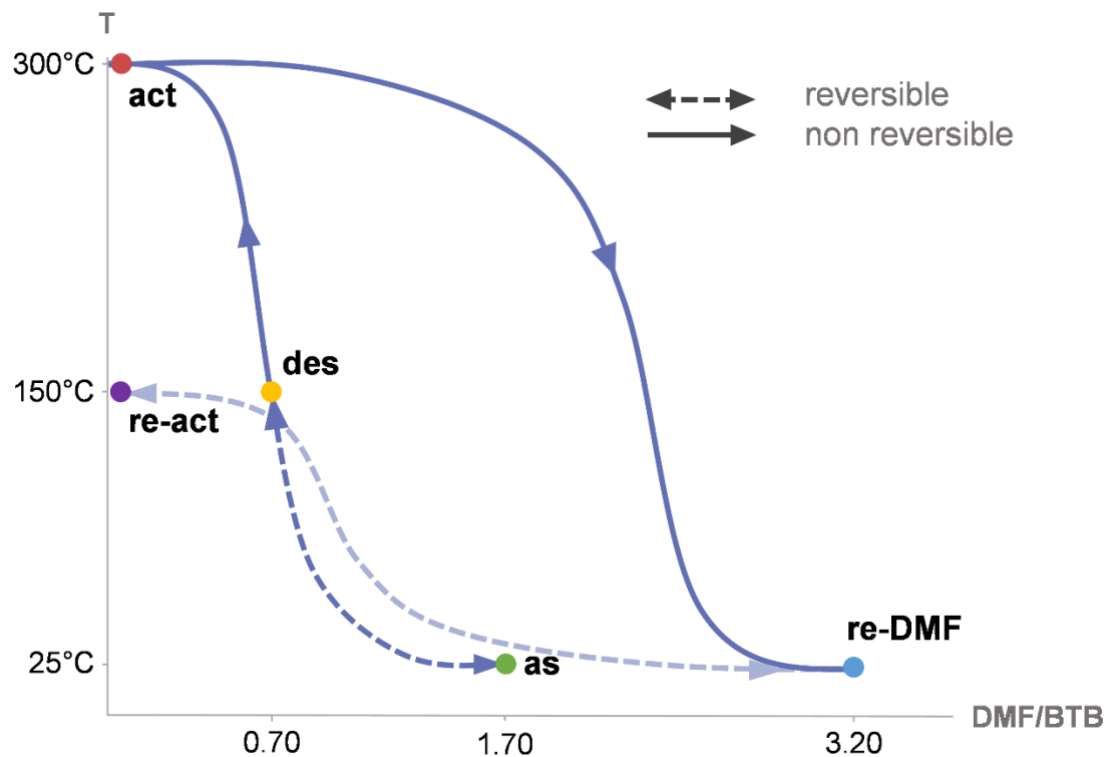


Figure S10. Schematic representation of the different phase transitions in the dynamic LOF structures.

S6. Thermogravimetric analysis

TGA was performed using a TGA 550 (TA Instruments) in high-resolution mode with a ramp of 20.0 °C/min from 25 to 600 °C under air atmosphere.

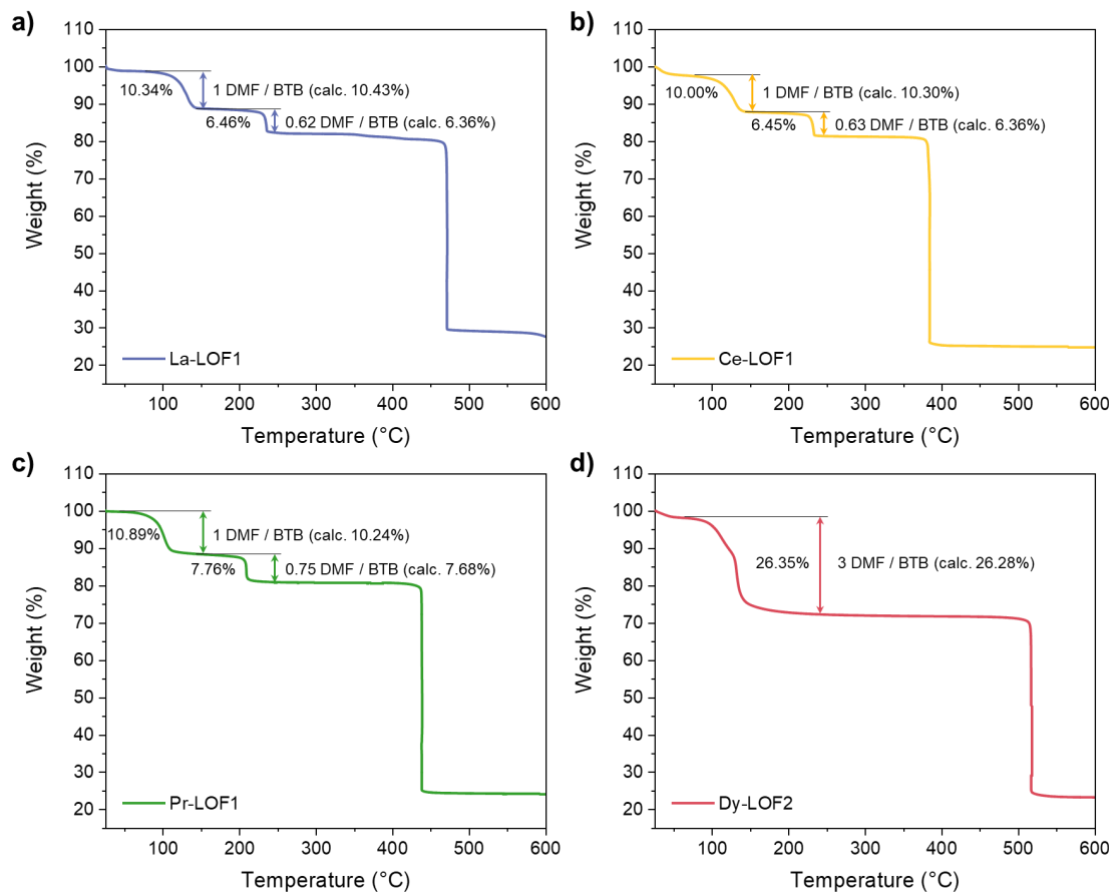


Figure S11. Thermogravimetric profiles of La-LOF1 (a), Ce-LOF1 (b), Pr-LOF1 (c), and Dy-LOF2 (d) and the corresponding comparison of the calculated and the experimental solvent losses.

In the case of LOF1 samples, the first mass loss (100-150 °C) can be attributed to the evaporation of the solvated DMF molecules (which corresponds to approximately 10% of mass). The second loss happens at approximately 200 °C (6-7%) and can be assigned to the removal of the coordinated DMF molecules. Finally, the last loss would correspond to the decomposition of the framework by the degradation of the BTB ligand. On the contrary, for LOF2 (Dy-LOF2), only one large loss of 26.35% is observed between 100-150 °C, also attributed to the removal of solvent molecules in the structure. Using La-LOF1 as an example: the DMF content was calculated based

on the assumption that the molecular formula of the structure above 300 °C corresponds to LaC₂₇H₁₅O₆ [La(BTB)] (574.31 g/mol). The first loss, which represents a 10.34% of the mass, implies a loss of 72.49 g/mol, matching the removal of 1 DMF in the LOF structure. The subsequent mass loss of 6.46% corresponds to a loss of 45.29 g/mol in the structure, which represents 0.62 DMF.

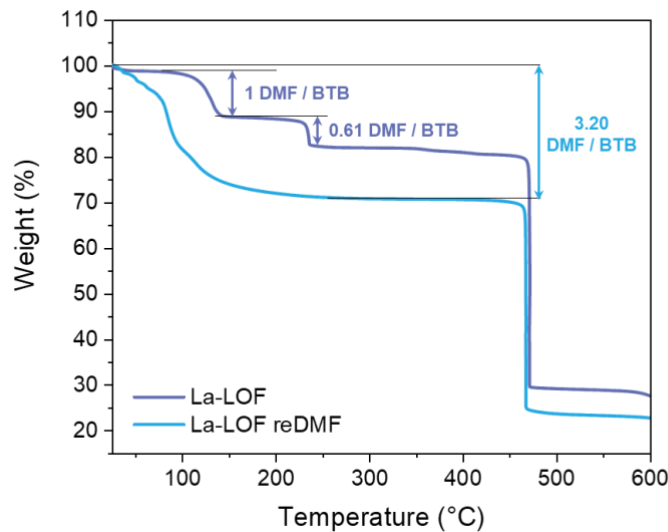


Figure S12. Thermogravimetric profiles of La-LOF1 and La-LOF1_reDMF and the assignment of the corresponding losses of DMF molecules.

In the TGA profile of **La-LOF1_reDMF**, no mass loss occurs at 225 °C, resulting in a similar profile to the rigid Dy-LOF2 form. In this case, the 29.25% mass loss represents a loss of 3.20 DMF/BTB.

S7. ^1H NMR spectroscopy

^1H NMR spectra were recorded using a Bruker DPX300 (300 MHz) spectrometer and Me₄Si as an internal standard. **La-LOF1_as**, **La-LOF1_des**, **La-LOF1_act**, and **La-LOF1_reDMF** were digested in DMSO with D₂SO₄ and the ratio DMF/BTB was calculated for each of them.

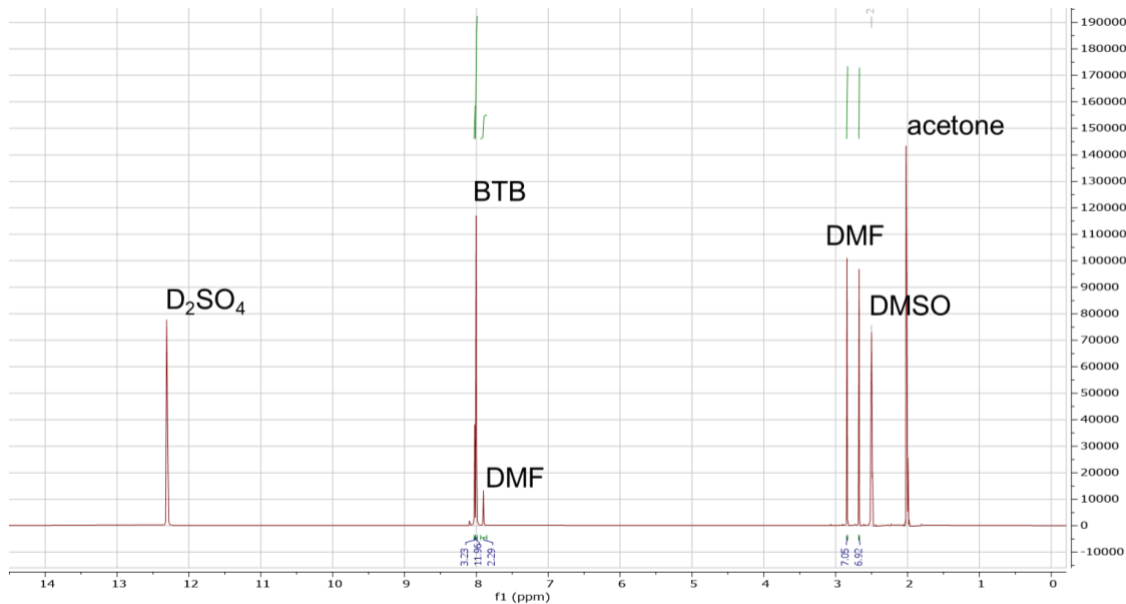


Figure S13. ^1H NMR spectrum of La-LOF1.



Figure S14. ^1H NMR spectrum of La-LOF1_des.

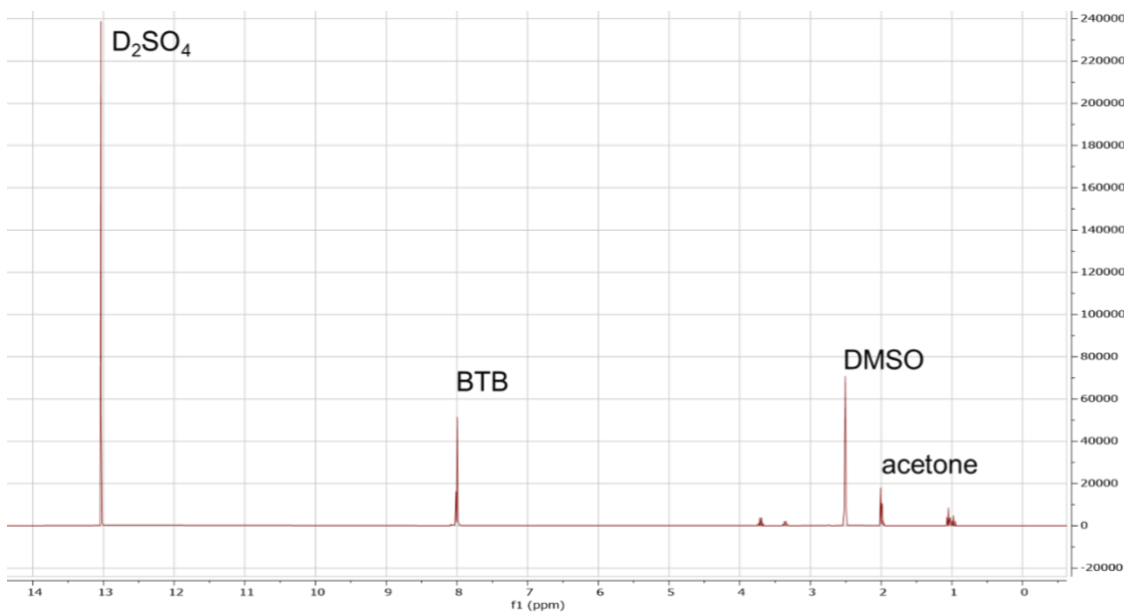


Figure S15. ¹H NMR spectrum of **La-LOF1_act**.

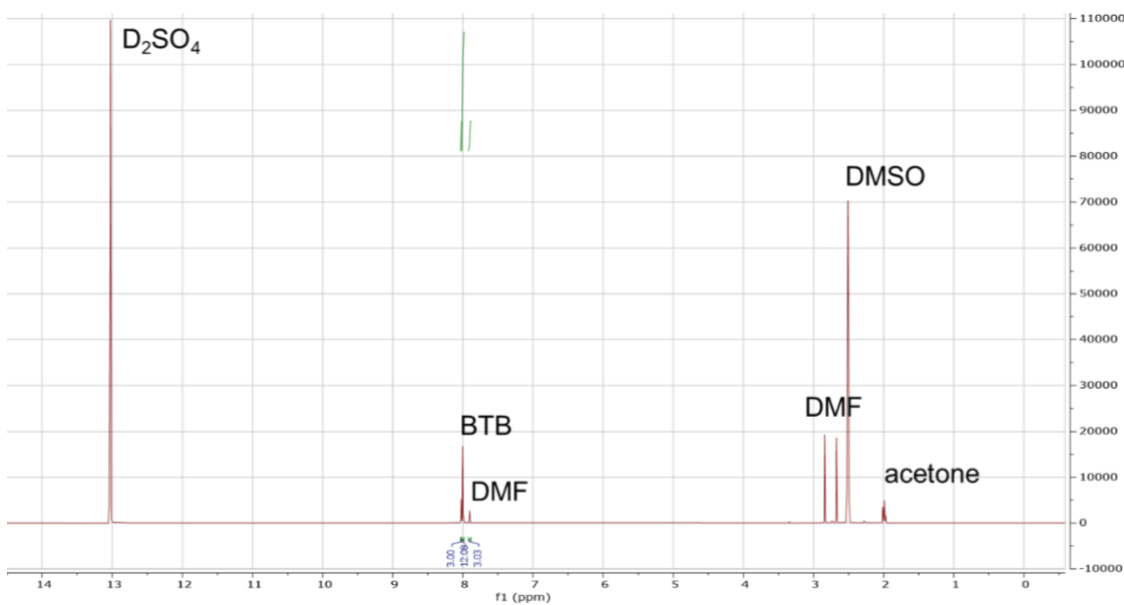


Figure S16. ¹H NMR spectrum of **La-LOF1_reDMF**.

Table S6. DMF content of each La-LOF1 structure expressed as DMF/BTB ligand calculated by TGA and ^1H NMR.

DMF/BTB	TGA	^1H NMR
La-LOF1_as	1.62	1.78
La-LOF1_des	0.62	0.67
La-LOF1_act	0.00	0.00
La-LOF1_reDMF	3.20	3.00

S8. Gas sorption measurements

Gas sorption measurements. Low-pressure N₂ and CO₂ sorption isotherms were recorded using a TRISTAR II instrument (Micromeritics) at 77 K and 273 K, respectively. High-pressure sorption measurements were performed in an IGA-100 (Hiden Isochem) at 10, 25, 40, and 50 °C. All samples were activated at 150 or 300 °C under vacuum for 5 hours prior to measuring.

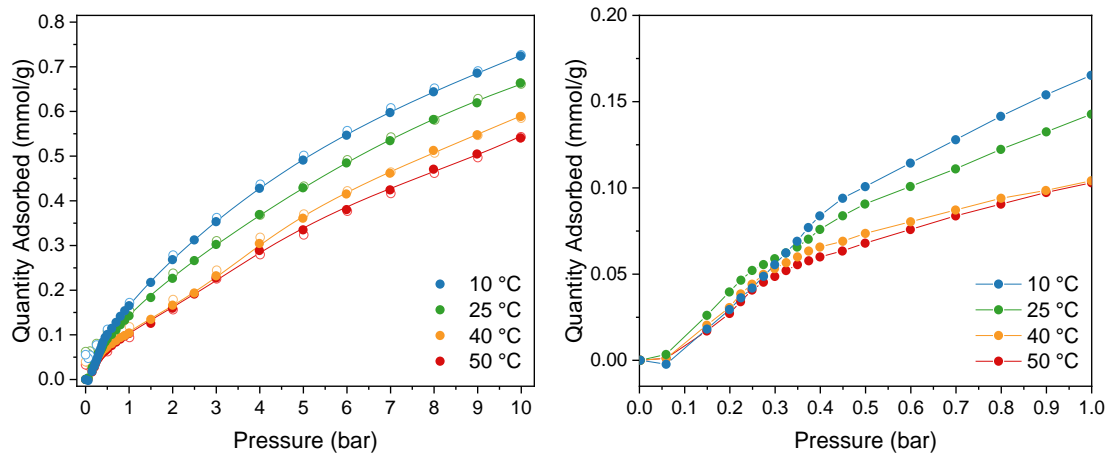


Figure S17. (Left) High-pressure N₂ adsorption-desorption isotherms at different temperatures (10-50 °C). Lines correspond to virial fitting. (Right) 0-1 bar zoom-in. In this case, only the adsorption branch is plotted and lines represent a guide for the eyes.

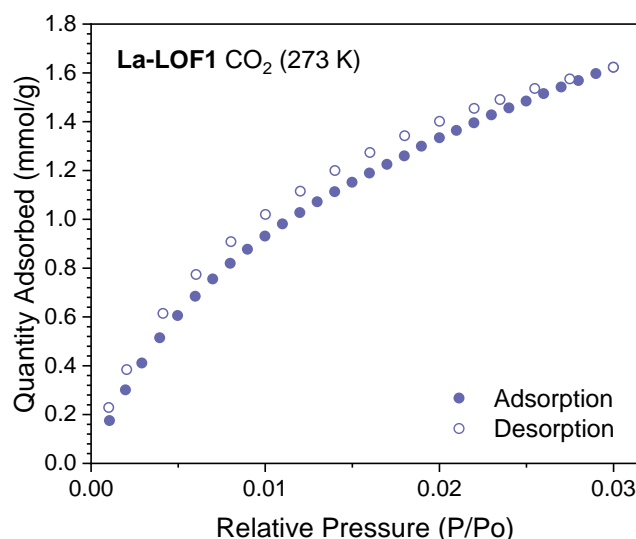


Figure S18. Low-pressure CO₂ adsorption-desorption isotherm performed at 273 K.

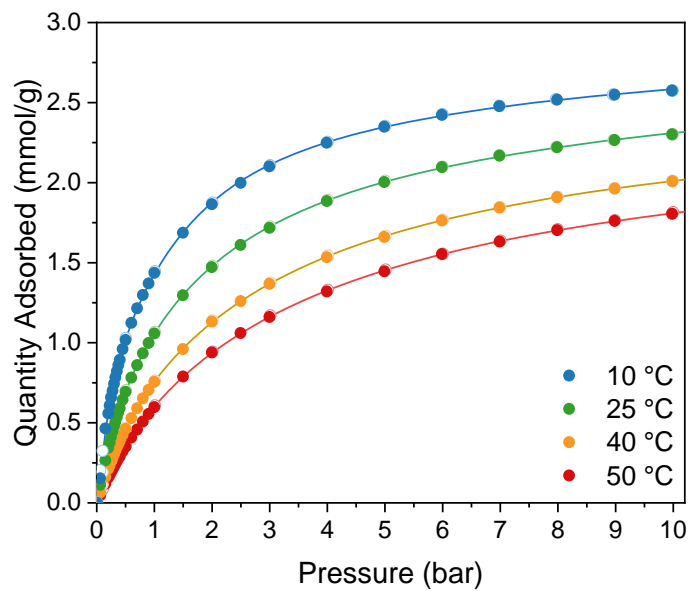


Figure S19. High-pressure CO₂ adsorption-desorption isotherms at different temperatures (10-50 °C). Lines correspond to fourth-grade polynomial virial approximation. Adsorption (solid symbols) and desorption (open) branches overlap.

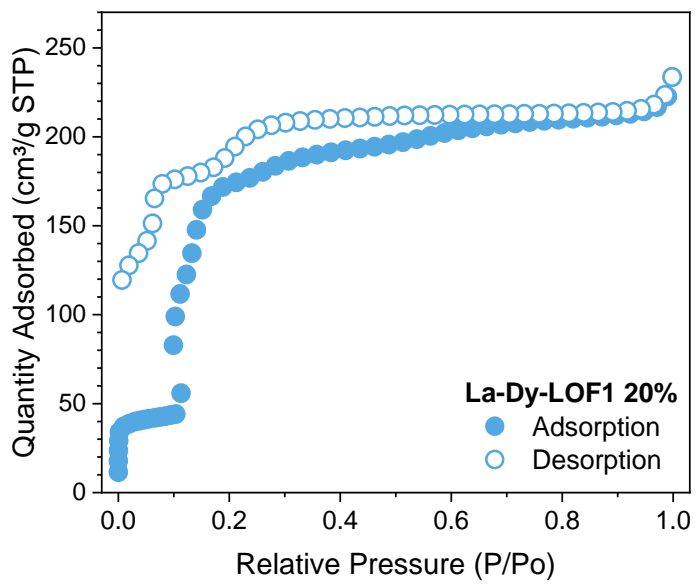


Figure S20. N₂ adsorption isotherms of **La-Dy-LOF1 20%**.

S9. AC and DC magnetic measurements

Magnetic measurements. The variable-temperature static magnetic susceptibilities were determined using an MPMS 3 SQUID magnetometer. Alternating current (AC) magnetic susceptibility measurements were performed at $f = 100\text{-}10000$ Hz and 2–15 K.

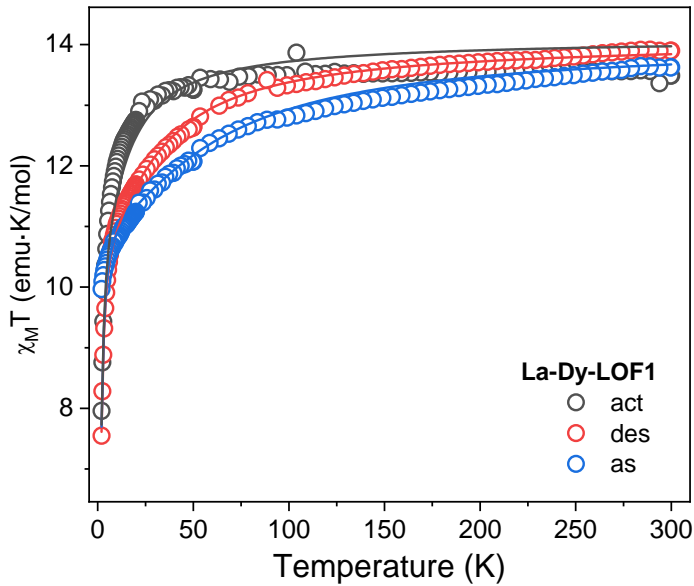


Figure S21. Experimental (symbols), fitted (solid line) temperature-dependence of the magnetic susceptibility from 2 to 300 K for **La-Dy-LOF1_as** (blue), **des** (red), and **act** (black).

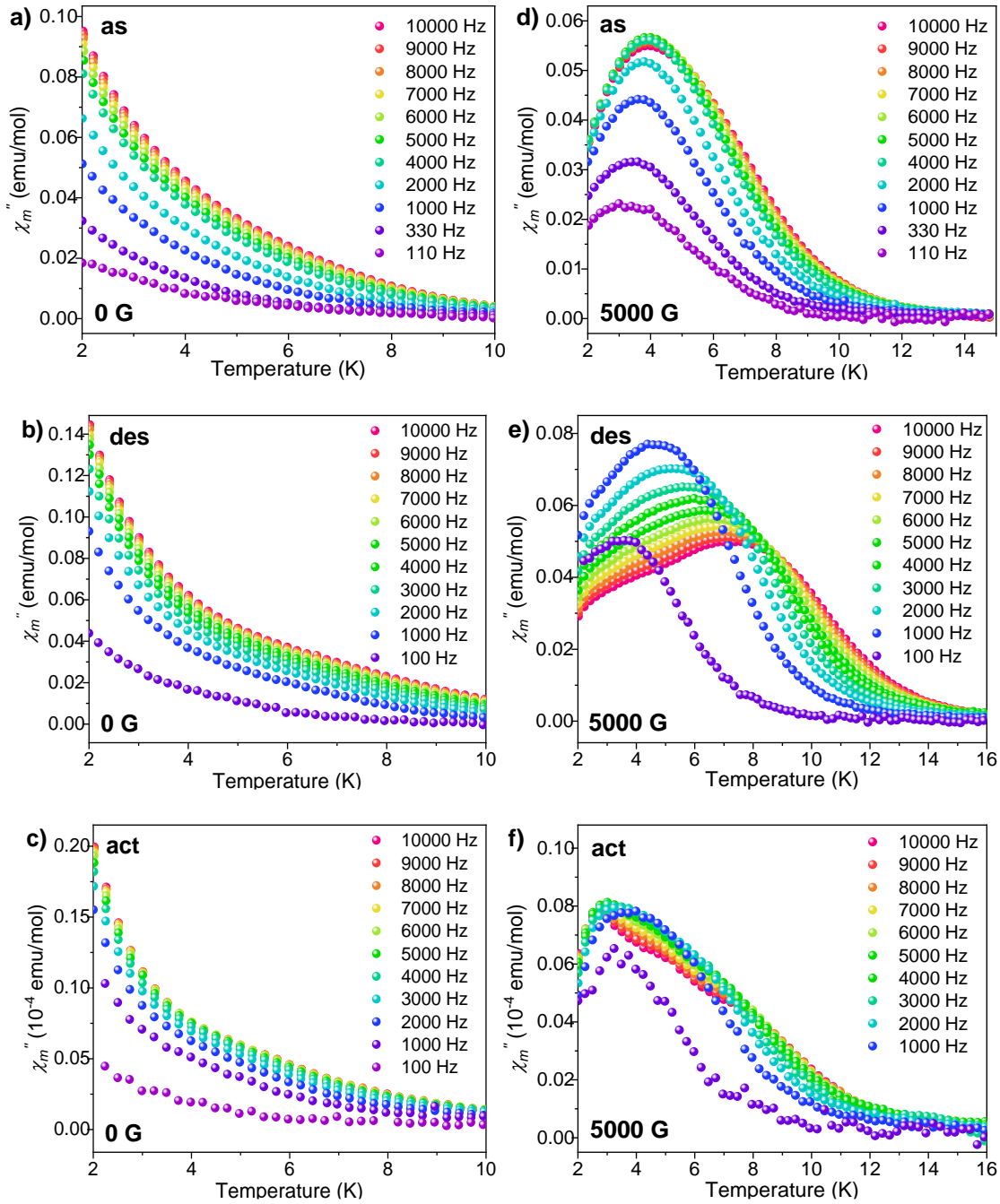


Figure S22. Temperature dependence of the out-of-phase signal χ'' of **La-Dy-LOF1_as** (a), **La-Dy-LOF1_des** (b) and **La-Dy-LOF1_act** (c) at different frequencies, under 0 G DC magnetic fields. Temperature dependence of the out-of-phase signal χ'' of **La-Dy-LOF1_as** (d), **La-Dy-LOF1_des** (e) and **La-Dy-LOF1_act** (f) at different frequencies, under 5000 G DC magnetic fields.

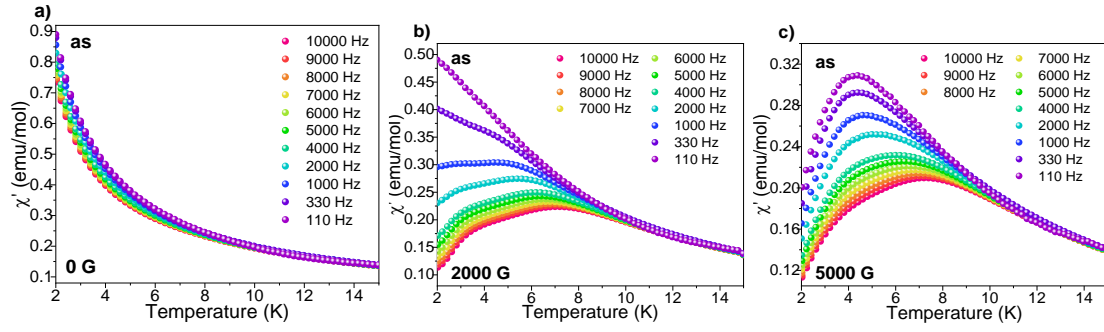


Figure S23. Temperature dependence of the in-phase signal χ' of La-Dy-LOF1_as under 0 G (a), 2000 G (b), and 5000 G (c) DC magnetic fields.

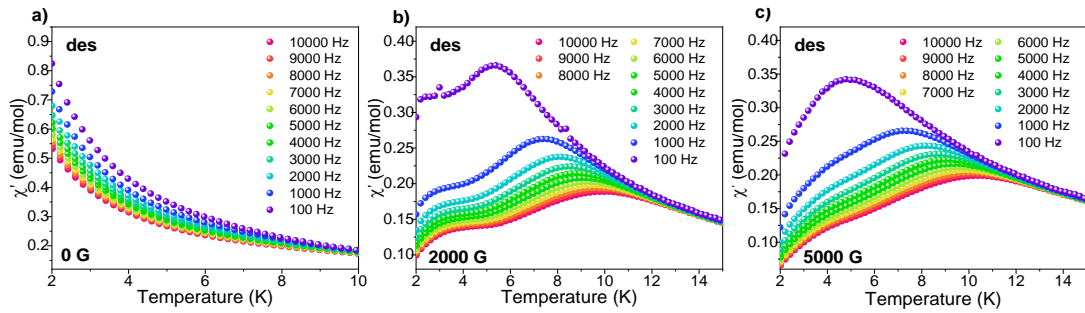


Figure S24. Temperature dependence of the in-phase signal χ' of La-Dy-LOF1_des under 0 G (a), 2000 G (b), and 5000 G (c) DC magnetic fields.

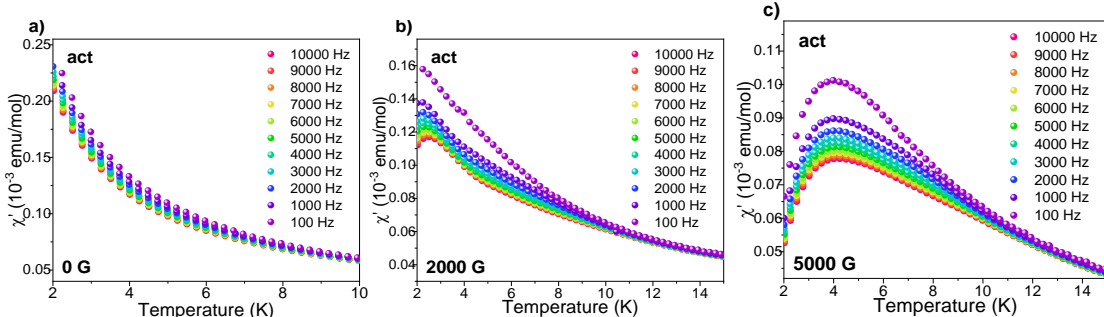


Figure S25. Temperature dependence of the in-phase signal χ' of La-Dy-LOF1_act under 0 G (a), 2000 G (b), and 5000 G (c) DC magnetic fields.

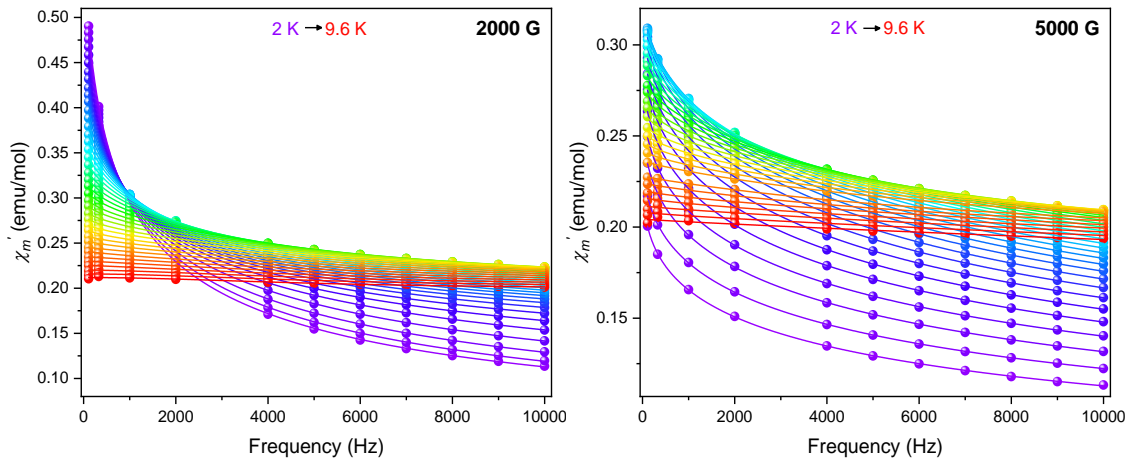


Figure S26. In-phase (χ') component of the magnetic susceptibility for **La-Dy-LOF1_as** under 2000 G (left) and 5000 G (right) dc fields. Solid lines correspond to the best fit obtained with a generalized Debye model.

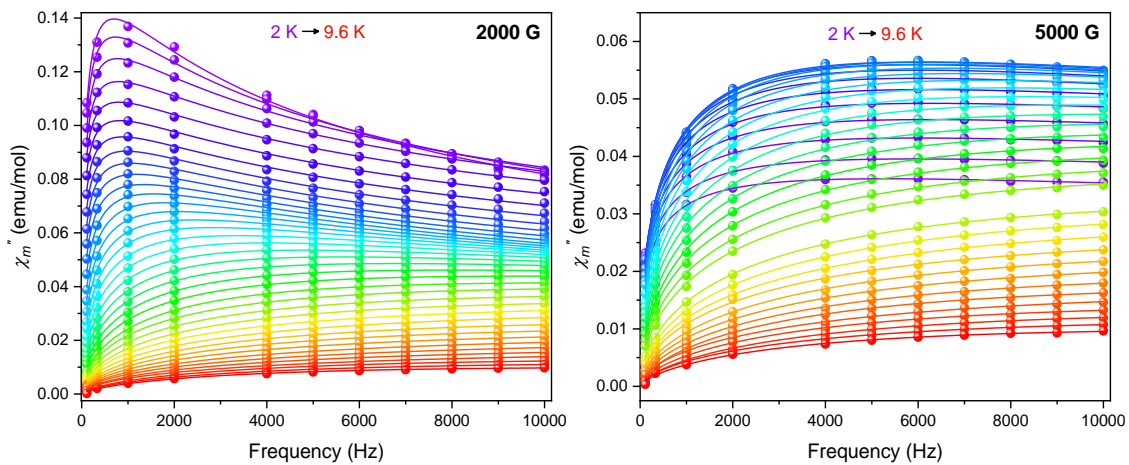


Figure S27. Out-of-phase (χ'') component of the magnetic susceptibility for **La-Dy-LOF1_as** under 2000 G (left) and 5000 G (right) dc fields. Solid lines correspond to the best fit obtained with a generalized Debye model.

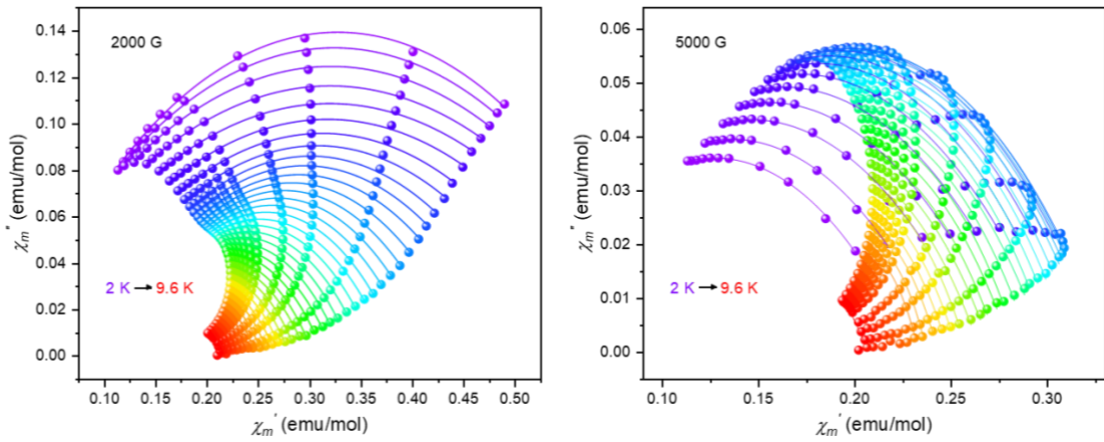


Figure S28. Cole-Cole plot for **La-Dy-LOF1_as** under 2000 G (left) and 5000 G (right) dc fields.

Solid lines correspond to the best fit obtained with a generalized Debye model.

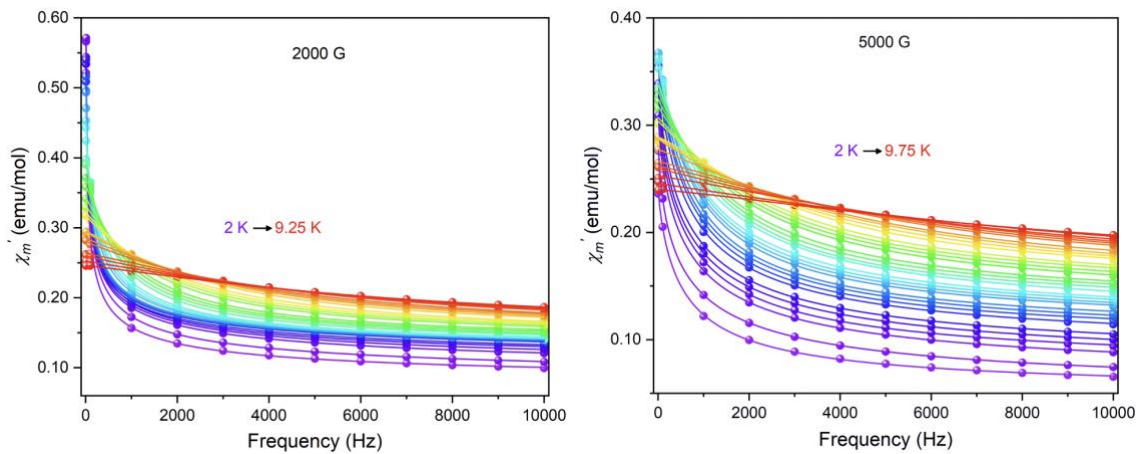


Figure S29. In-phase (χ') component of the magnetic susceptibility for **La-Dy-LOF1_des** under 2000 G (left) and 5000 G (right) dc fields. Solid lines correspond to the best fit obtained with a generalized Debye model.

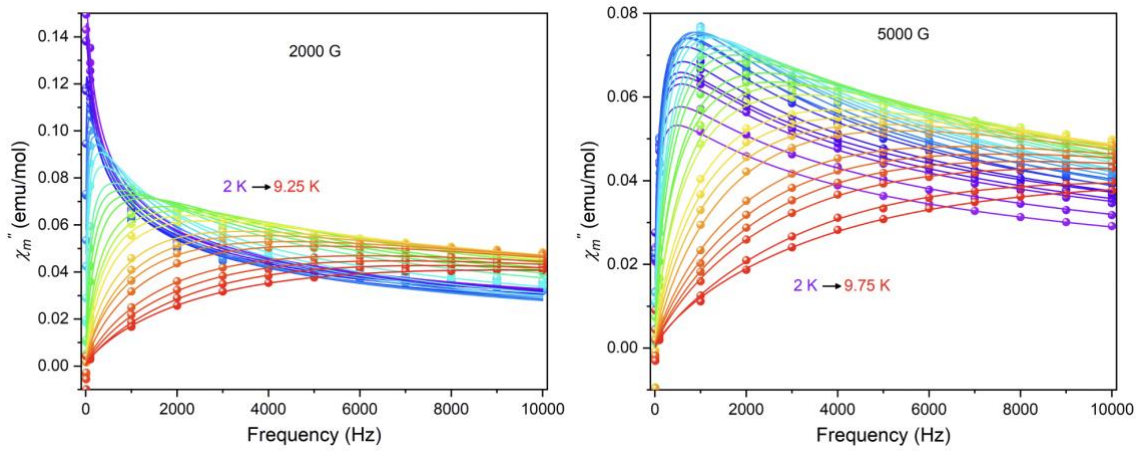


Figure S30. Out-of-phase (χ'') component of the magnetic susceptibility for **La-Dy-LOF1_des** under 2000 G (left) and 5000 G (right) dc fields. Solid lines correspond to the best fit obtained with a generalized Debye model.

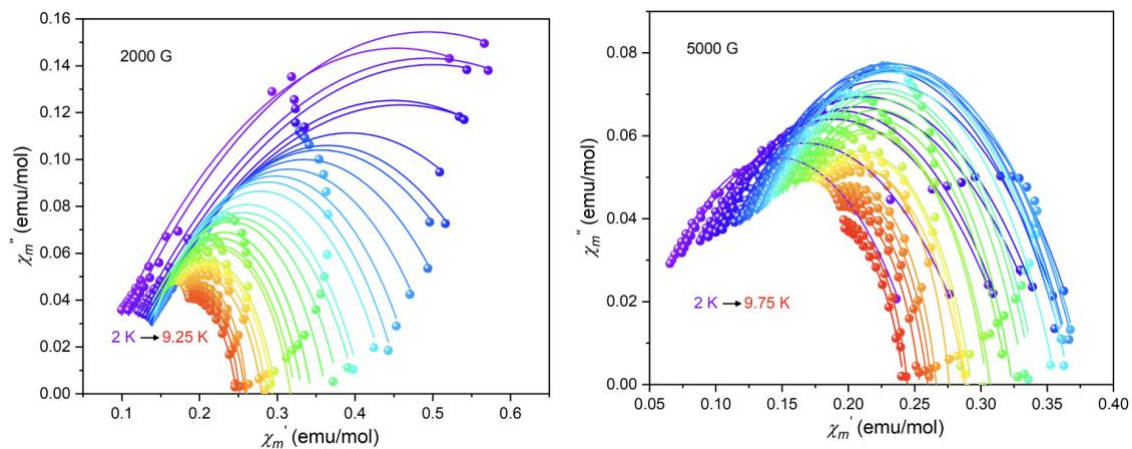


Figure S31. Cole-Cole plot for **La-Dy-LOF1_des** under 2000 G (left) and 5000 G (right) dc fields. Solid lines correspond to the best fit obtained with a generalized Debye model.

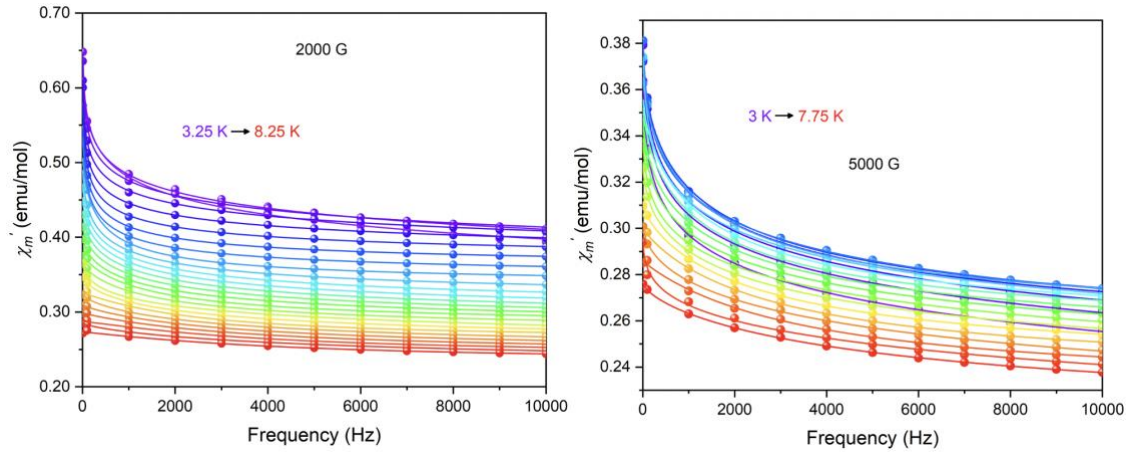


Figure S32. In-phase (χ') component of the magnetic susceptibility for **La-Dy-LOF1_act** under 2000 G (left) and 5000 G (right) dc fields. Solid lines correspond to the best fit obtained with a generalized Debye model.

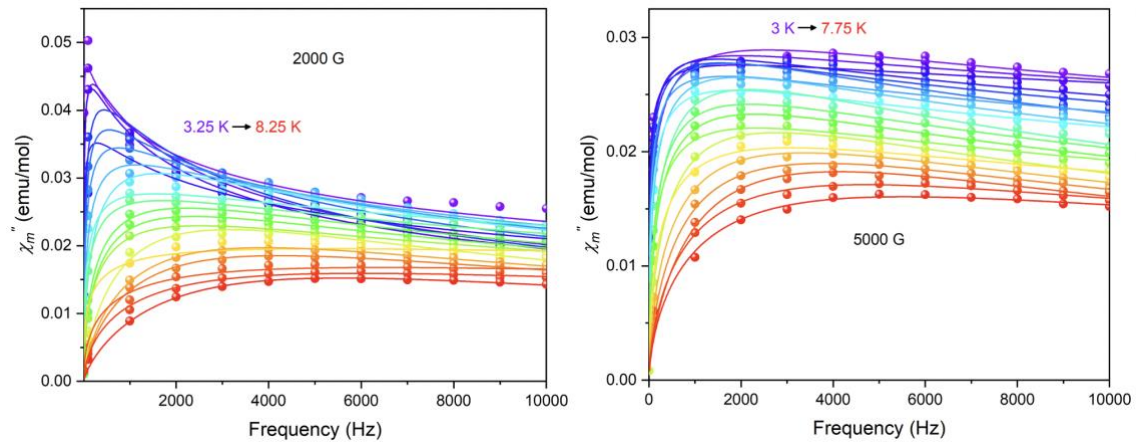


Figure S33. Out-of-phase (χ'') component of the magnetic susceptibility for **La-Dy-LOF1_act** under 2000 G (left) and 5000 G (right) dc fields. Solid lines correspond to the best fit obtained with a generalized Debye model.

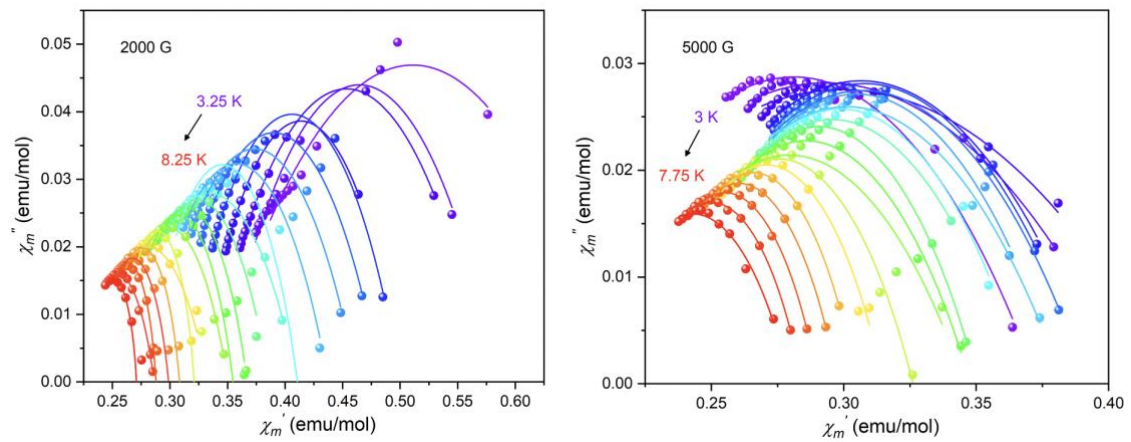


Figure S34. Cole-Cole plot for **La-Dy-LOF1_act** under 2000 G (left) and 5000 G (right) dc fields.

Solid lines correspond to the best fit obtained with a generalized Debye model.

Table S7. Cole-Cole fit values for **La-Dy-LOF1_as** under 2000 G (left) and 5000 G (right) dc fields.

2000 G					5000 G				
T/K	$\chi_i/\text{emu mol}^{-1}$	$\chi_s/\text{emu mol}^{-1}$	α	τ/s	T/K	$\chi_i/\text{emu mol}^{-1}$	$\chi_s/\text{emu mol}^{-1}$	α	τ/s
2.00	6.43E-01	1.26E-02	4.70E-01	2.29E-04	2.00	2.29E-01	2.55E-02	5.66E-01	3.00E-05
2.20	6.44E-01	5.36E-03	4.98E-01	2.19E-04	2.20	2.47E-01	2.45E-02	5.66E-01	2.69E-05
2.40	6.42E-01	5.06E+00	5.28E-01	2.06E-04	2.40	2.66E-01	2.64E-02	5.60E-01	2.65E-05
2.60	6.39E-01	1.50E-03	5.55E-01	2.00E-04	2.60	2.80E-01	2.98E-02	5.48E-01	2.56E-05
2.80	6.26E-01	1.40E-02	5.66E-01	1.98E-04	2.80	2.94E-01	3.33E-02	5.40E-01	2.54E-05
3.00	6.03E-01	3.25E-02	5.64E-01	1.92E-04	3.00	3.05E-01	3.95E-02	5.28E-01	2.58E-05
3.20	5.73E-01	5.24E-02	5.51E-01	1.79E-04	3.20	3.11E-01	5.23E-02	4.99E-01	2.67E-05
3.40	5.48E-01	6.83E-02	5.40E-01	1.65E-04	3.40	3.19E-01	5.48E-02	4.97E-01	2.65E-05
3.60	5.20E-01	8.35E-02	5.21E-01	1.50E-04	3.60	3.24E-01	6.09E-02	4.88E-01	2.67E-05
3.80	4.98E-01	9.38E-02	5.10E-01	1.35E-04	3.80	3.28E-01	6.48E-02	4.85E-01	2.66E-05
4.00	4.78E-01	1.02E-01	4.98E-01	1.19E-04	4.00	3.31E-01	6.64E-02	4.87E-01	2.54E-05
4.20	4.55E-01	1.10E-01	4.81E-01	1.03E-04	4.20	3.30E-01	7.32E-02	4.76E-01	2.53E-05
4.40	4.35E-01	1.17E-01	4.65E-01	8.87E-05	4.40	3.29E-01	7.33E-02	4.80E-01	2.40E-05
4.60	4.19E-01	1.21E-01	4.56E-01	7.63E-05	4.60	3.26E-01	7.84E-02	4.73E-01	2.29E-05
4.80	4.03E-01	1.24E-01	4.47E-01	6.54E-05	4.80	3.24E-01	7.87E-02	4.79E-01	2.14E-05
5.00	3.90E-01	1.26E-01	4.42E-01	5.59E-05	5.00	3.18E-01	8.54E-02	4.66E-01	2.02E-05
5.20	3.78E-01	1.25E-01	4.46E-01	4.71E-05	5.20	3.13E-01	8.88E-02	4.62E-01	1.91E-05
5.40	3.66E-01	1.27E-01	4.40E-01	3.99E-05	5.40	3.08E-01	9.17E-02	4.58E-01	1.70E-05
5.60	3.54E-01	1.26E-01	4.42E-01	3.33E-05	5.60	3.03E-01	9.60E-02	4.53E-01	1.54E-05
5.80	3.42E-01	1.29E-01	4.33E-01	2.81E-05	5.80	2.99E-01	8.72E-02	4.78E-01	1.35E-05
6.00	3.33E-01	1.27E-01	4.39E-01	2.35E-05	6.00	2.92E-01	9.67E-02	4.60E-01	1.24E-05
6.20	3.24E-01	1.24E-01	4.49E-01	1.99E-05	6.20	2.86E-01	1.05E-01	4.44E-01	1.14E-05
6.40	3.14E-01	1.27E-01	4.41E-01	1.66E-05	6.40	2.82E-01	9.77E-02	4.67E-01	9.23E-06
6.60	3.04E-01	1.30E-01	4.32E-01	1.46E-05	6.60	2.76E-01	1.01E-01	4.63E-01	8.34E-06
6.80	2.98E-01	1.25E-01	4.50E-01	1.15E-05	6.80	2.71E-01	9.70E-02	4.78E-01	7.98E-06
7.00	2.88E-01	1.35E-01	4.25E-01	1.05E-05	7.00	2.66E-01	9.85E-02	4.77E-01	6.22E-05
7.20	2.81E-01	1.34E-01	4.33E-01	9.39E-06	7.20	2.59E-01	1.27E-01	4.22E-01	7.42E-06
7.40	2.74E-01	1.39E-01	4.29E-01	7.30E-06	7.40	2.54E-01	1.28E-01	4.27E-01	6.46E-06
7.60	2.68E-01	1.35E-01	4.43E-01	6.88E-06	7.60	2.49E-01	1.34E-01	4.20E-01	6.15E-07
7.80	2.60E-01	1.51E-01	4.02E-01	7.32E-06	7.80	2.43E-01	1.49E-01	3.79E-01	6.38E-06
8.00	2.54E-01	1.57E-01	3.94E-01	7.02E-06	8.00	2.37E-01	1.60E-01	3.32E-01	6.74E-06
8.20	2.47E-01	1.69E-01	3.49E-01	6.38E-06	8.20	2.33E-01	1.62E-01	3.35E-01	6.59E-06
8.40	2.43E-01	1.64E-01	3.81E-01	5.33E-06	8.40	4.18E-01	4.18E-01	6.34E-01	7.22E-06
8.60	2.37E-01	1.77E-01	3.20E-01	4.71E-06	8.60	4.71E-01	4.71E-01	7.21E-01	8.49E-06
8.80	2.32E-01	1.79E-01	3.10E-01	5.81E-06	8.80	5.13E-01	5.13E-01	7.69E-01	5.56E-06
9.00	2.27E-01	1.81E-01	2.95E-01	4.70E-06	9.00	4.97E-01	4.97E-01	8.57E-01	8.22E-06
9.20	2.22E-01	1.70E-01	3.60E-01	9.20E-06	9.20	3.94E-01	3.94E-01	8.37E-01	8.38E-06
9.40	2.18E-01	1.61E-01	4.16E-01	8.84E-06	9.40	3.65E-01	3.65E-01	8.60E-01	8.10E-06
9.60	2.14E-01	1.45E-01	4.70E-01	1.15E-05	9.60	2.07E-01	7.83E-02	5.39E-01	1.01E-05

Table S8. Cole-Cole fit values for **La-Dy-LOF1_des** under 2000 G (left) and 5000 G (right) dc fields.

2000 G					5000 G				
T/K	$\chi^u/\text{emu mol}^{-1}$	$\chi^s/\text{emu mol}^{-1}$	α	τ/s	T/K	$\chi^u/\text{emu mol}^{-1}$	$\chi^s/\text{emu mol}^{-1}$	α	τ/s
2.00	8.52E-01	5.70E-02	5.48E-01	9.52E-03	2.00	2.57E-01	3.61E-02	4.14E-01	3.23E-04
2.25	9.21E-01	6.47E-02	5.59E-01	5.13E-03	2.25	2.99E-01	3.54E-02	4.71E-01	2.86E-04
2.50	9.13E-01	7.43E-02	5.81E-01	5.13E-03	2.50	3.30E-01	4.73E-02	4.59E-01	2.74E-04
2.75	9.23E-01	7.83E-02	5.91E-01	5.16E-03	2.75	3.31E-01	5.64E-02	4.29E-01	2.58E-04
3.00	8.38E-01	8.05E-02	5.99E-01	5.07E-03	3.00	3.59E-01	5.49E-02	4.72E-01	2.80E-04
3.25	8.09E-01	8.93E-02	5.74E-01	5.06E-03	3.25	3.62E-01	6.28E-02	4.47E-01	2.59E-04
3.50	6.87E-01	9.87E-02	5.39E-01	3.31E-03	3.50	3.74E-01	7.34E-02	4.23E-01	2.36E-04
3.75	6.26E-01	1.04E-01	5.09E-01	1.83E-03	3.75	3.68E-01	8.26E-02	3.79E-01	2.10E-04
4.00	6.05E-01	1.06E-01	4.98E-01	1.84E-03	4.00	3.83E-01	8.10E-02	4.10E-01	2.26E-04
4.25	5.61E-01	1.09E-01	4.69E-01	1.16E-03	4.25	3.72E-01	8.99E-02	3.60E-01	1.88E-04
4.50	5.18E-01	1.11E-01	4.40E-01	8.57E-04	4.50	3.76E-01	9.37E-02	3.63E-01	1.69E-04
4.75	4.82E-01	1.14E-01	4.05E-01	6.28E-04	4.75	3.79E-01	9.36E-02	3.73E-01	1.61E-04
5.00	4.61E-01	1.14E-01	3.88E-01	4.84E-04	5.00	3.70E-01	9.77E-02	3.53E-01	1.46E-04
5.25	4.44E-01	1.13E-01	3.87E-01	4.11E-04	5.25	3.67E-01	1.00E-01	3.46E-01	1.30E-04
5.50	4.10E-01	1.13E-01	3.66E-01	2.50E-04	5.50	3.57E-01	1.04E-01	3.36E-01	1.07E-04
5.75	4.02E-01	1.11E-01	3.78E-01	2.01E-04	5.75	3.43E-01	1.08E-01	3.05E-01	9.82E-05
6.00	3.81E-01	1.14E-01	3.47E-01	1.57E-04	6.00	3.39E-01	1.11E-01	2.98E-01	8.95E-05
6.25	3.63E-01	1.18E-01	3.13E-01	1.24E-04	6.25	3.33E-01	1.13E-01	2.88E-01	8.06E-05
6.50	3.44E-01	1.20E-01	2.97E-01	9.14E-05	6.50	3.24E-01	1.19E-01	2.68E-01	6.63E-05
6.75	3.32E-01	1.22E-01	2.84E-01	7.90E-05	6.75	3.20E-01	1.19E-01	2.80E-01	6.14E-05
7.00	3.23E-01	1.22E-01	2.83E-01	7.00E-05	7.00	3.07E-01	1.21E-01	2.57E-01	5.36E-05
7.25	3.17E-01	1.25E-01	2.66E-01	6.05E-05	7.25	3.04E-01	1.26E-01	2.40E-01	4.89E-05
7.50	2.98E-01	1.25E-01	2.58E-01	4.65E-05	7.50	2.93E-01	1.25E-01	2.47E-01	3.93E-05
7.75	2.93E-01	1.29E-01	2.44E-01	4.09E-05	7.75	2.89E-01	1.32E-01	2.19E-01	3.55E-05
8.00	2.86E-01	1.29E-01	2.42E-01	3.58E-05	8.00	2.88E-01	1.22E-01	2.80E-01	3.20E-05
8.25	2.80E-01	1.26E-01	2.61E-01	3.18E-05	8.25	2.76E-01	1.43E-01	1.53E-01	2.94E-05
8.50	2.61E-01	1.43E-01	1.44E-01	2.58E-05	8.50	2.66E-01	1.37E-01	1.84E-01	2.38E-05
8.75	2.59E-01	1.31E-01	2.26E-01	2.32E-05	8.75	2.63E-01	1.37E-01	1.89E-01	2.11E-05
9.00	2.51E-01	1.42E-01	1.60E-01	2.11E-05	9.00	2.60E-01	1.30E-01	2.31E-01	1.96E-05
9.25	2.47E-01	1.31E-01	2.22E-01	1.74E-05	9.25	2.54E-01	1.35E-01	2.01E-01	1.73E-05

Table S9. Cole-Cole fit values for **La-Dy-LOF1_act** under 2000 G (left) and 5000 G (right) dc fields.

2000 G					5000 G				
T/K	χ' /emu mol ⁻¹	χ'' /emu mol ⁻¹	α	τ /s	T/K	χ' /emu mol ⁻¹	χ'' /emu mol ⁻¹	α	τ /s
3.25	6.85E-01	3.37E-01	6.64E-01	2.26E-03	3.00	3.73E-01	1.89E-01	6.15E-01	6.17E-05
3.50	5.85E-01	3.44E-01	5.55E-01	8.00E-04	3.25	4.08E-01	1.78E-01	6.94E-01	7.99E-05
3.75	5.75E-01	3.31E-01	5.65E-01	8.99E-04	3.50	4.24E-01	1.74E-01	7.23E-01	8.13E-05
4.00	5.02E-01	3.25E-01	4.76E-01	5.48E-04	3.75	3.97E-01	2.16E-01	6.13E-01	1.05E-04
4.25	5.00E-01	3.12E-01	4.92E-01	3.62E-04	4.00	3.93E-01	2.22E-01	5.95E-01	1.03E-04
4.50	4.83E-01	2.97E-01	5.20E-01	2.88E-04	4.25	3.92E-01	2.22E-01	6.01E-01	9.32E-05
4.75	4.62E-01	2.85E-01	5.27E-01	2.10E-04	4.50	3.82E-01	2.28E-01	5.70E-01	9.51E-05
5.00	4.38E-01	2.77E-01	5.13E-01	1.39E-04	4.75	3.83E-01	2.19E-01	6.08E-01	8.28E-05
5.25	4.11E-01	2.81E-01	4.16E-01	9.84E-05	5.00	3.69E-01	2.29E-01	5.51E-01	8.57E-05
5.50	4.11E-01	2.58E-01	5.52E-01	1.03E-04	5.25	3.66E-01	2.25E-01	5.69E-01	7.32E-05
5.75	3.86E-01	2.62E-01	4.78E-01	9.28E-05	5.50	3.51E-01	2.30E-01	5.15E-01	7.27E-05
6.00	3.67E-01	2.62E-01	4.17E-01	7.21E-05	5.75	3.48E-01	2.23E-01	5.54E-01	6.90E-05
6.25	3.55E-01	2.60E-01	3.89E-01	6.69E-05	6.00	3.46E-01	2.13E-01	6.02E-01	6.75E-05
6.50	3.50E-01	2.47E-01	4.69E-01	6.34E-05	6.25	3.26E-01	2.25E-01	5.00E-01	5.77E-05
6.75	3.21E-01	2.57E-01	2.24E-01	5.05E-05	6.50	3.15E-01	2.27E-01	4.47E-01	5.17E-05
7.00	3.33E-01	2.29E-01	5.32E-01	4.32E-05	6.75	3.05E-01	2.26E-01	4.05E-01	4.72E-05
7.25	3.08E-01	2.44E-01	2.97E-01	4.09E-05	7.00	2.98E-01	2.23E-01	4.08E-01	4.19E-05
7.50	2.99E-01	2.36E-01	3.26E-01	3.76E-05	7.25	2.90E-01	2.20E-01	4.01E-01	3.86E-05
7.75	2.88E-01	2.39E-01	2.03E-01	2.46E-05	7.50	2.84E-01	2.16E-01	4.15E-01	3.38E-05
8.00	2.86E-01	2.23E-01	4.09E-01	2.65E-05	7.75	2.80E-01	2.06E-01	4.82E-01	2.88E-05
8.25	2.71E-01	2.31E-01	1.73E-01	2.85E-05					

Table S10. Fitting parameters of the extracted relaxation times for **La-Dy-LOF1_as**, **La-Dy-LOF1_des** and **La-Dy-LOF1_act** compounds.

	La-Dy-LOF1_as	La-Dy-LOF1_des	La-Dy-LOF1_act
$\tau_{\text{QTM}} / 10^{-3} \text{ s}$	0.22(2)	9.8(4)	-
$C / 10^{-4} \text{ s}^{-1} \text{ K}^{-n}$	22(4)	0.40(11)	-
n	9	9	-
$\tau_0 / 10^{-6} \text{ s}$	2.5(9)	0.90(14)	1.40(17)
$U_{\text{eff}} / \text{K}$	19(1)	31.3(8)	24.0(6)

S10. Qubit properties

EPR measurements. X-band continuous-wave and pulsed EPR data were recorded on an ELEXSYS E580 EPR spectrometer (Bruker) equipped with a pulsed X-band (9.70 GHz cavity and resonators) operating in the range 4–300 K. The CW EPR powder spectra were simulated by EasySpin toolbox³⁷ (<http://www.easyspin.org/>) based on Matlab. Field-swept electron spin echo-detected EPR spectra were recorded using a two-pulse echo sequence ($\pi/2-\tau-\pi-\tau$ -echo) with micro-wave pulse lengths of 16 ns and 32 ns and an interpulse time $\tau = 200$ ns. The echo decay curves were collected by application of the abovementioned sequence at the field of maximum echo intensity at variable temperatures with varying τ (starting from $\tau = 200$ ns). T1 values were obtained at the main resonances using a three-pulse inversion recovery sequence ($\pi-T-\pi/2-\tau-\pi-\tau$ -echo) with $\tau = 500$ ns and with the four-step phase cycling. Rabi oscillations were performed using a variable-length nutation pulse (tp) within the standard sequence (tp-T- $\pi/2-\tau-\pi-\tau$ -echo) at different attenuations of the microwave power. For the measurements performed in the presence of N₂, the tube with the sample was first prepared in a glovebox assuring a N₂ atmosphere and later a balloon filled with N₂ was attached to the lid of the tube with a hypodermic needle.

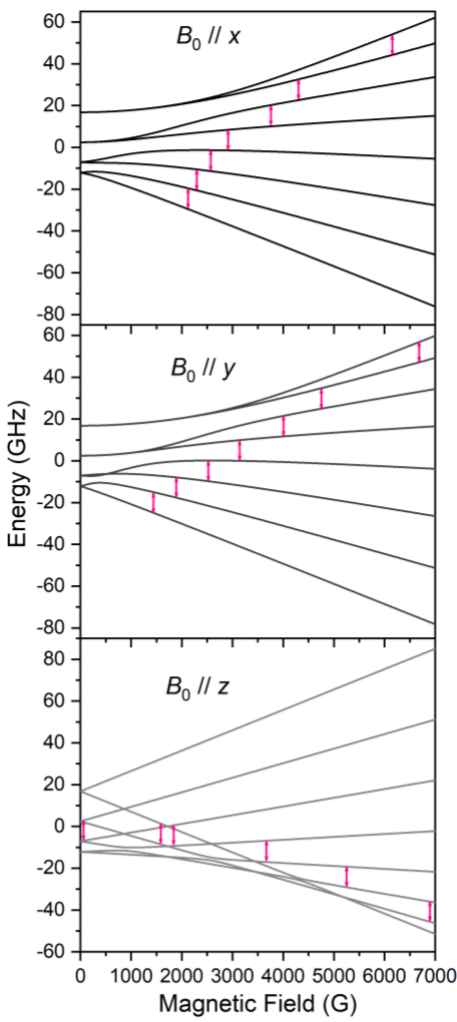


Figure S35. Zeeman diagrams for **La-Gd-LOF1_act** sample.

Table S11. Simulation parameters for **La-Gd-LOF1 act**, **des**, and **as** samples extracted from the EDFS analysis.

Sample	g_{iso}	$D (\text{cm}^{-1})$	$E (\text{cm}^{-1})$
Act	1.99	0.080	0.0035
Des	1.99	0.055	0.0025
As	1.99	0.038	0.010

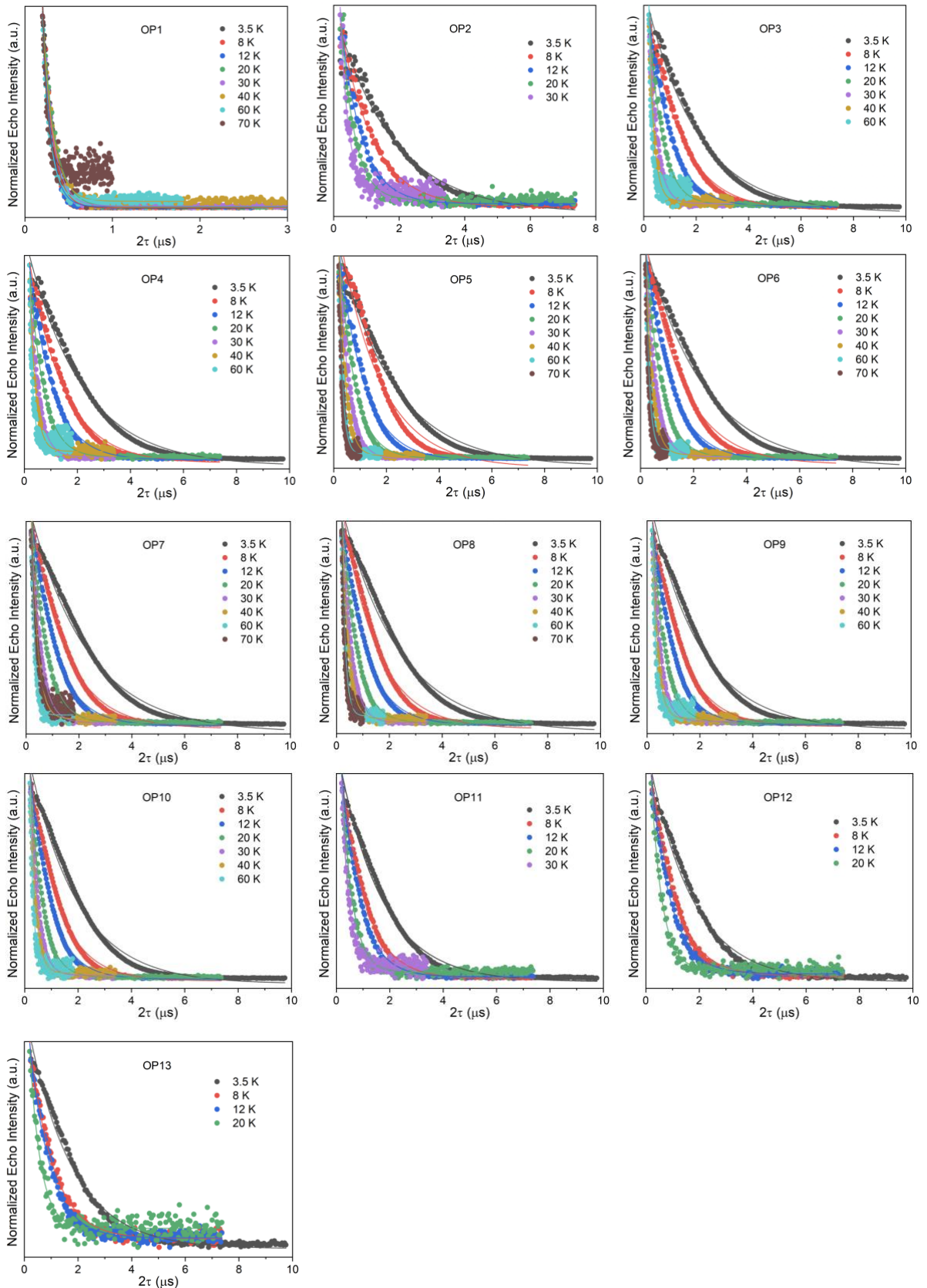


Figure S36. T_2 curves of La-Gd-LOF1_act measured at OP1-13 at different temperatures.

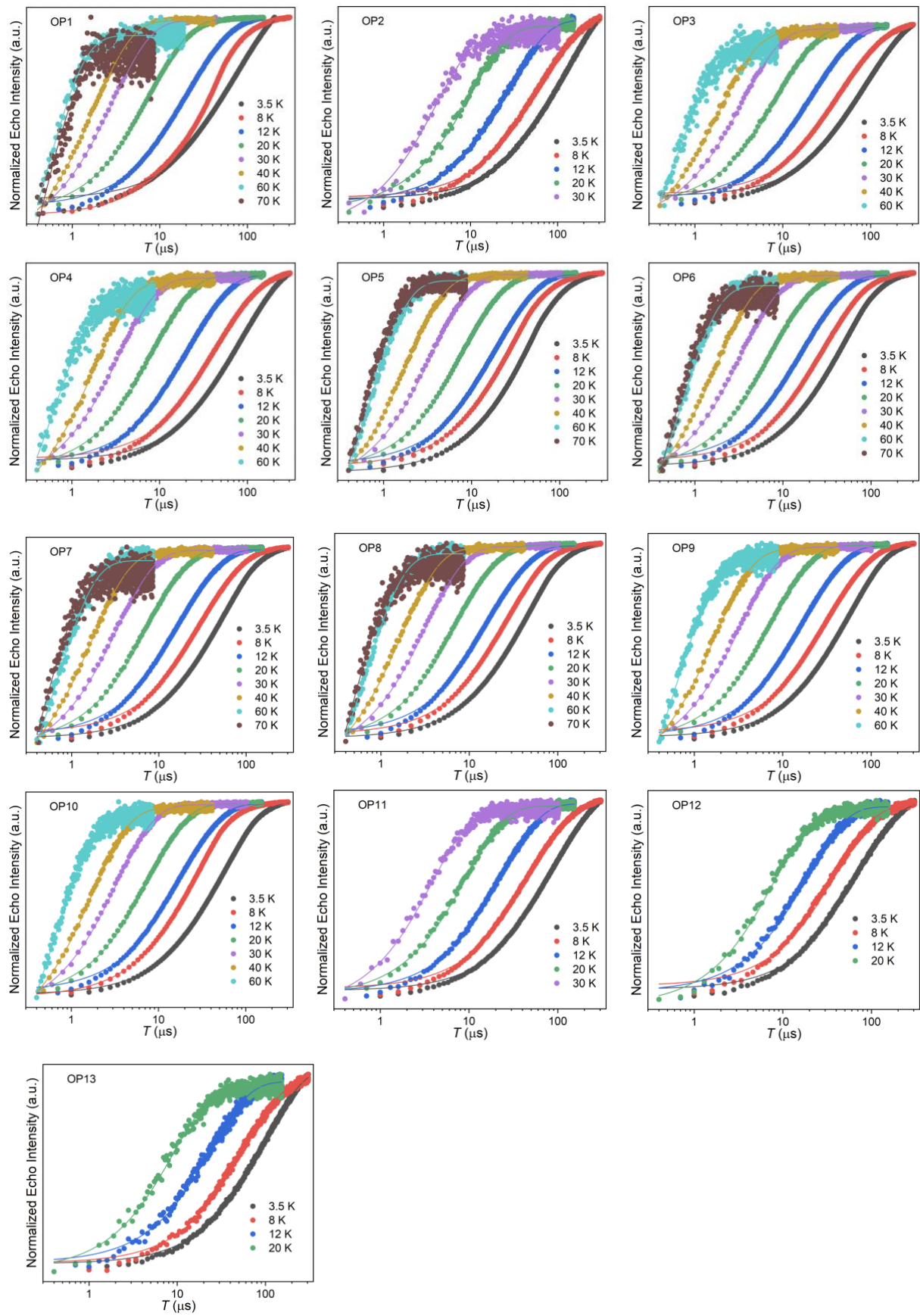


Figure S37. T_1 curves of **La-Gd-LOF1_act** measured at OP1-13 at different temperatures.

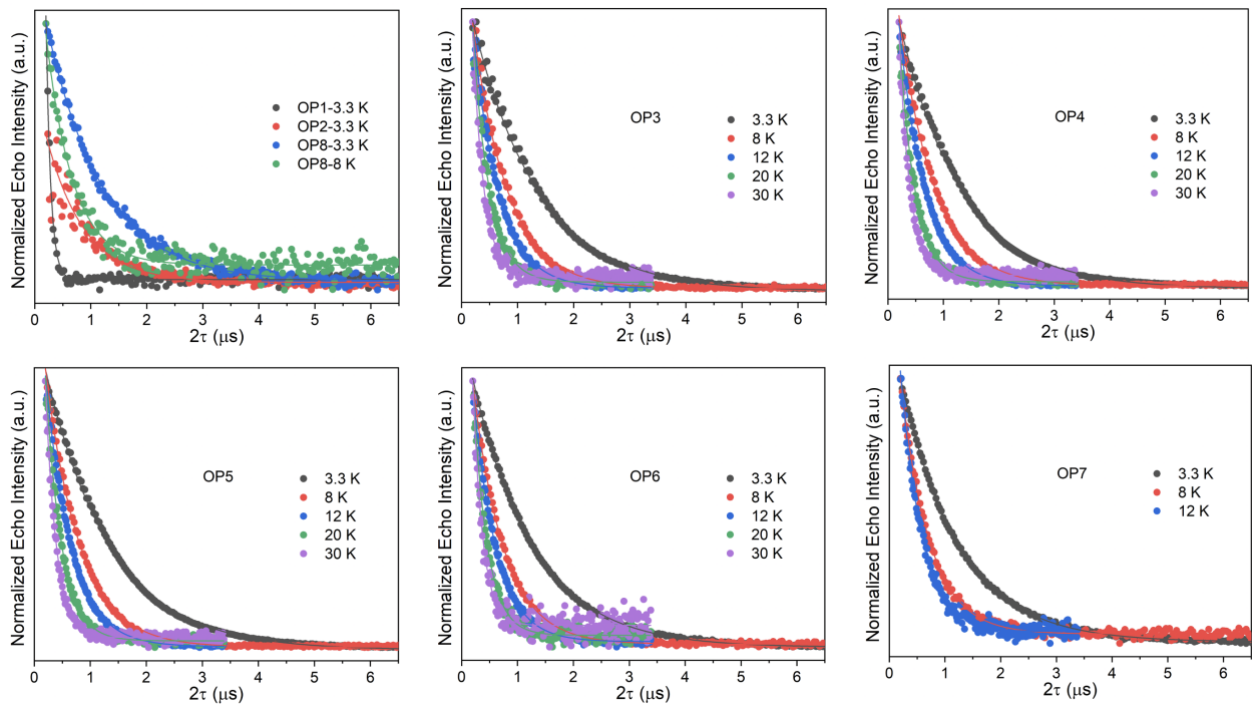


Figure S38. T_2 curves of **La-Gd-LOF1_des** measured at OP1-8 at different temperatures.

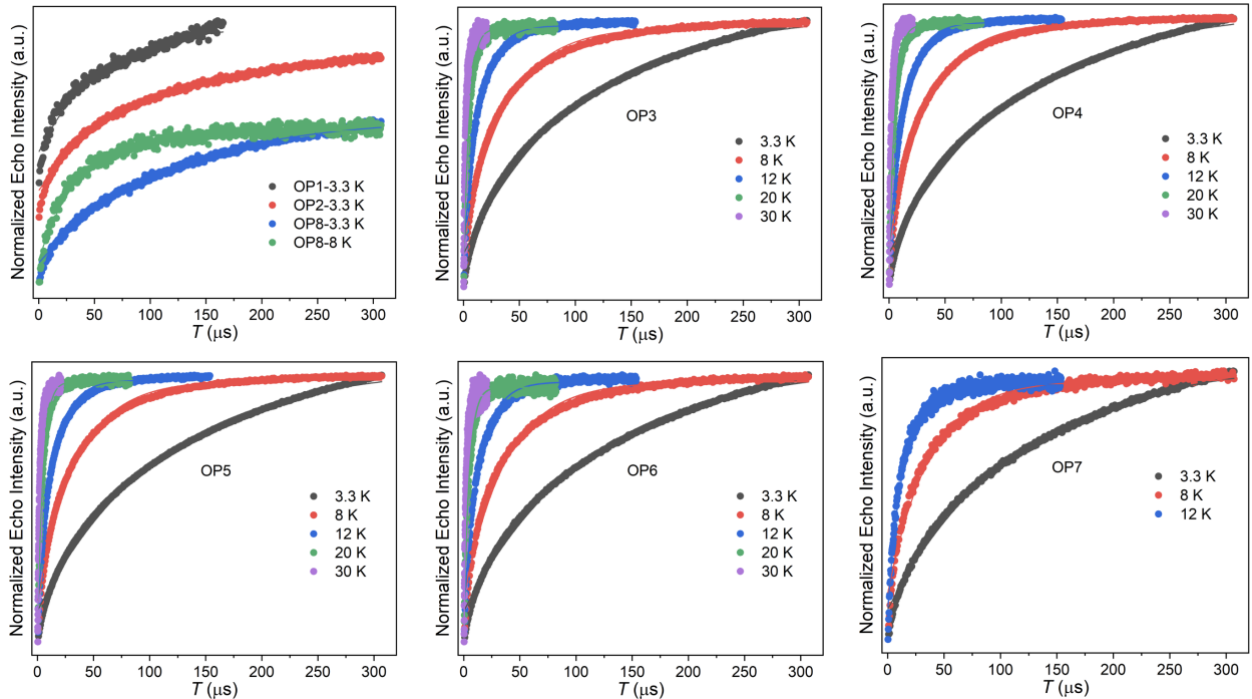


Figure S39. T_1 curves of **La-Gd-LOF1_des** measured at OP1-8 at different temperatures.

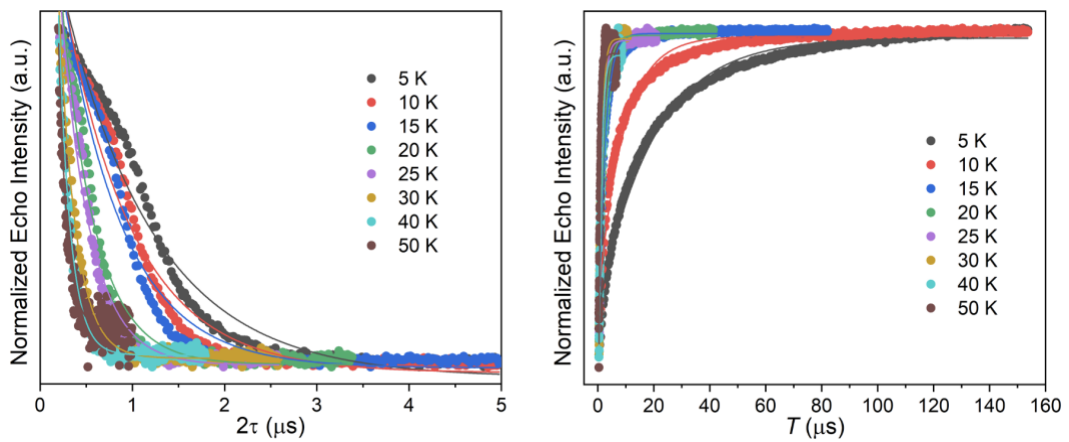


Figure S40. T_2 (left) and T_1 curves (right) of **La-Gd-LOF1_as** measured at OP1 at different temperatures.

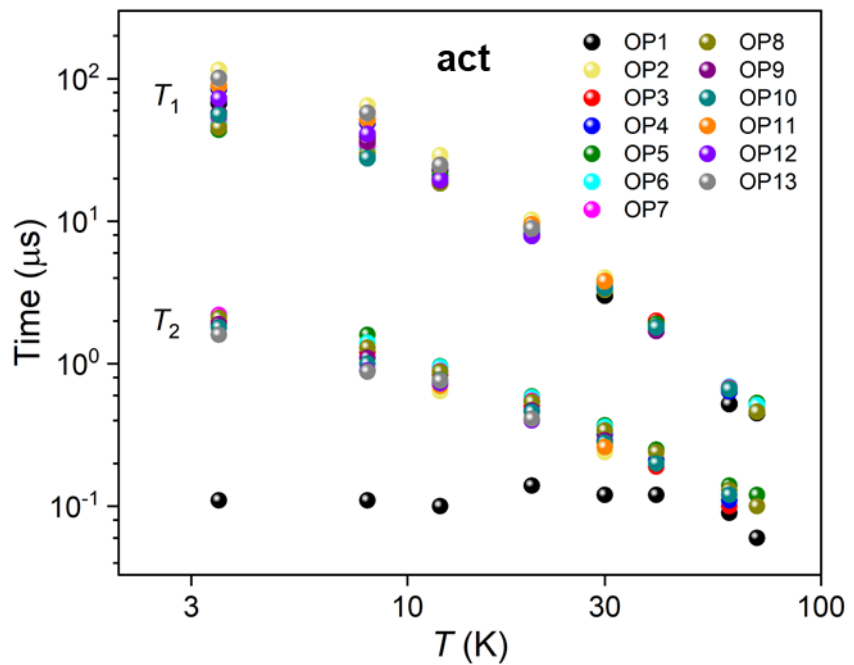


Figure S41. Temperature dependence of T_1 and T_2 at different OPs for **La-Gd-LOF1_act**.

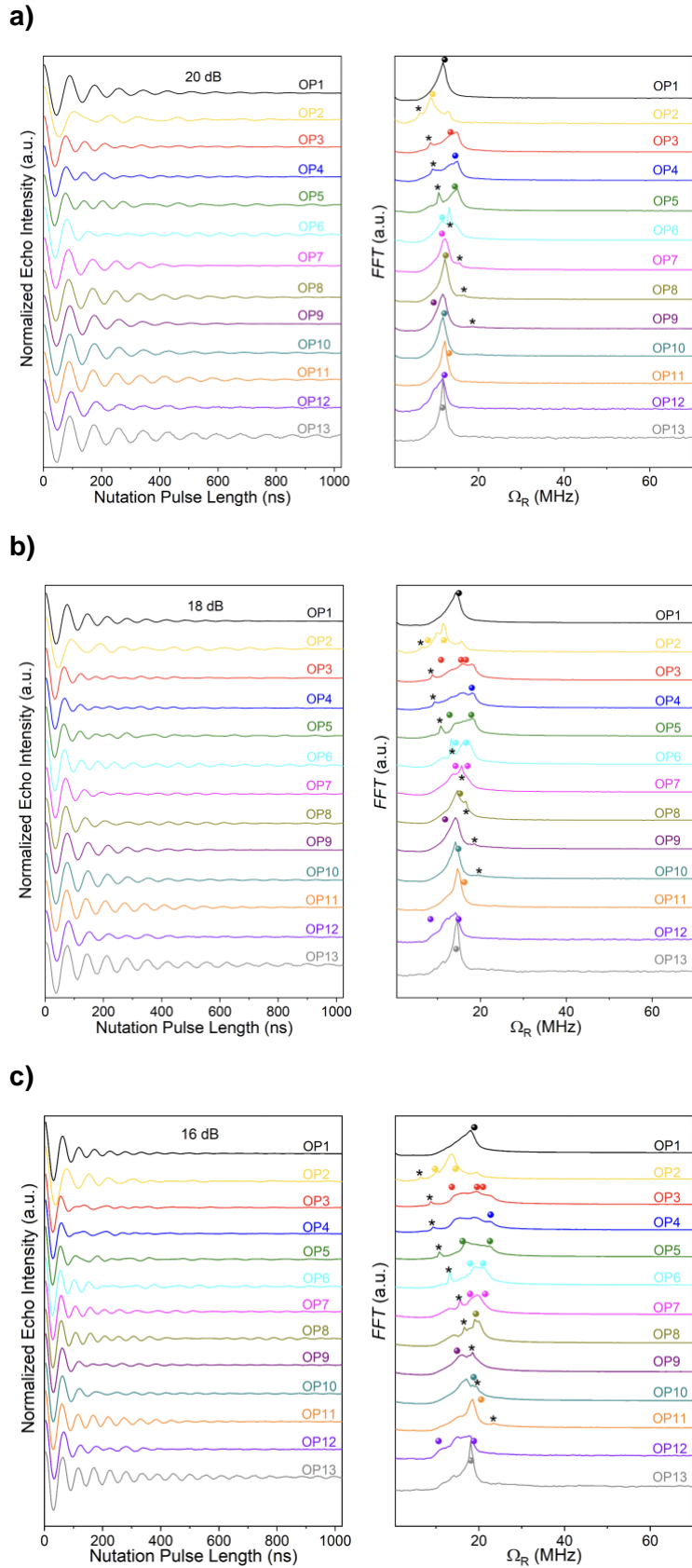
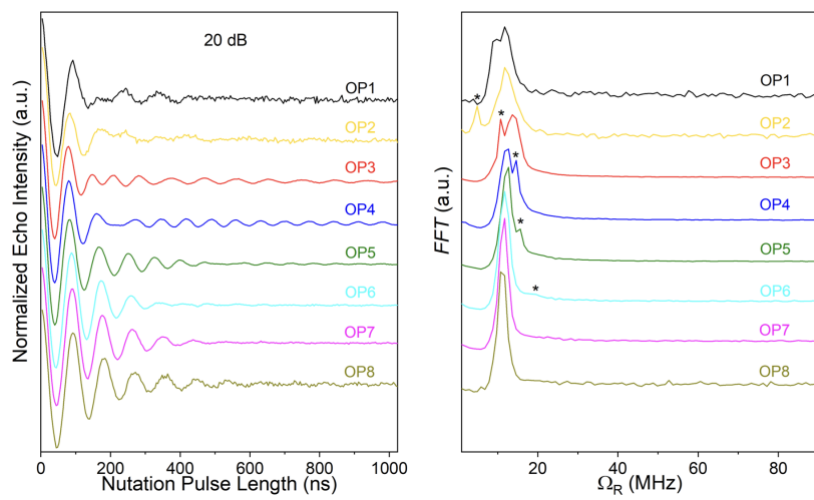
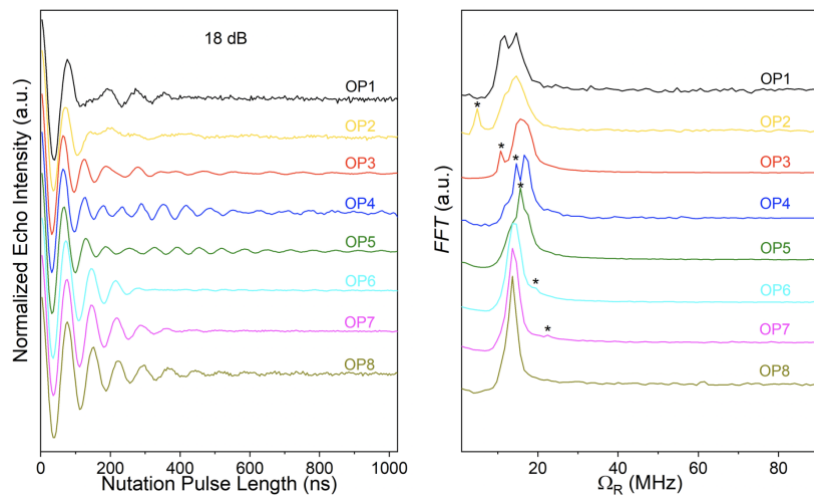


Figure S42. (Left) Rabi oscillations of La-Gd-LOF1_act at 3.5 K using different microwave powers for OP1-8: 20 dB (a), 18 dB (b), and 16 dB (c). (Right) their corresponding Fourier transforms. The stars indicate the Larmor frequency of H nuclei.

a)



b)



c)

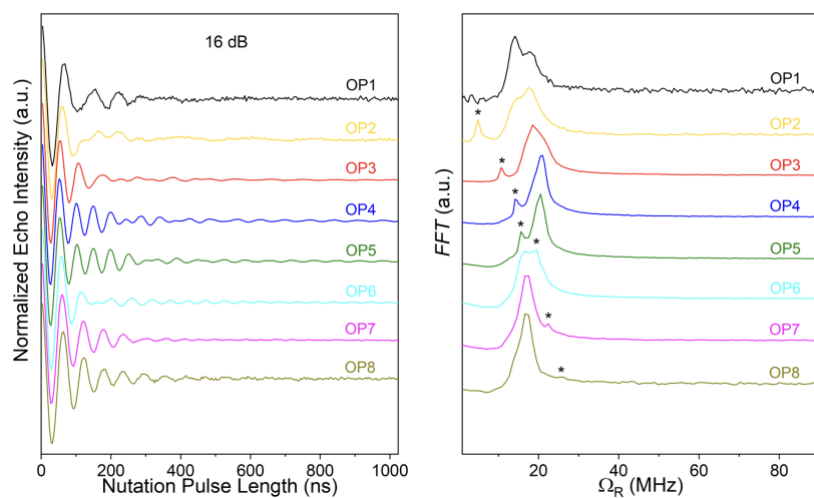


Figure S43. (Left) Rabi oscillations of **La-Gd-LOF1_des** at 3.3 K using different microwave powers for OP1-8: 20 dB (a), 18 dB (b), and 16 dB (c). (Right) their corresponding Fourier transforms. The stars indicate the Larmor frequency of H nuclei.

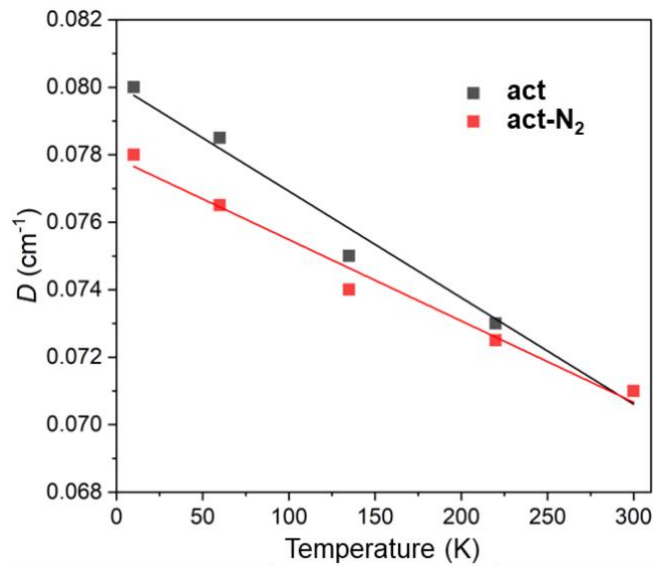


Figure S44. Temperature dependence of D for **La-Gd-LOF1_act** and **La-Gd-LOF1_act-N₂**.

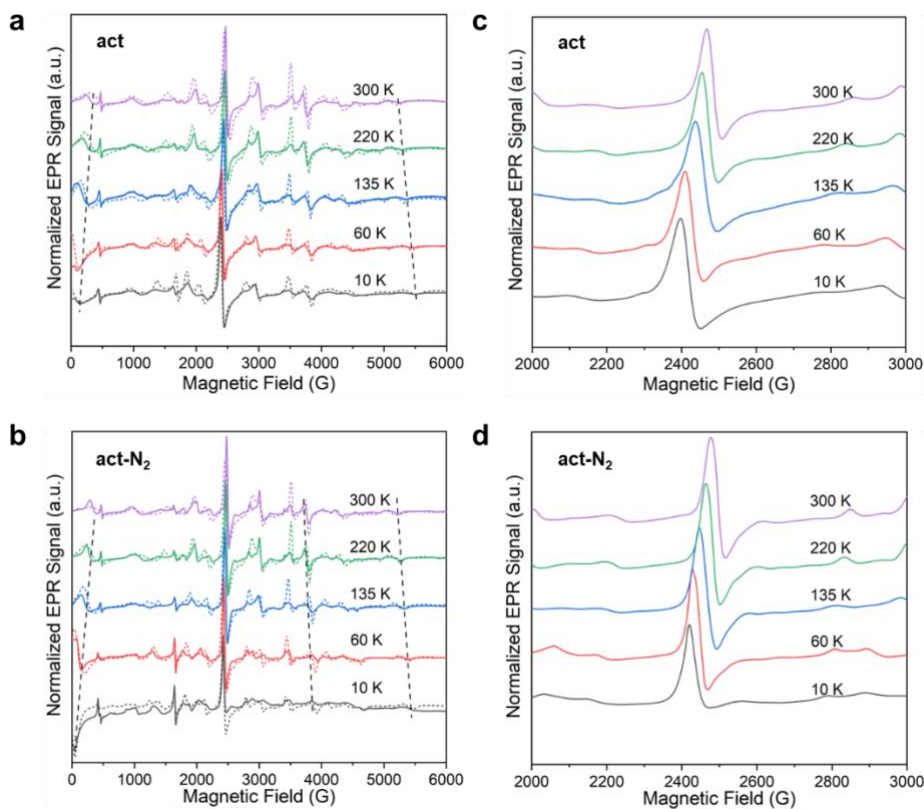


Figure S45. Variable-temperature CW EPR spectra of **La-Gd-LOF1_act** (a) and **La-Gd-LOF1_act-N₂** (b) and their corresponding zoom-in between 2000 and 3000 G (c, d). The dashed lines represent the simulated spectra.

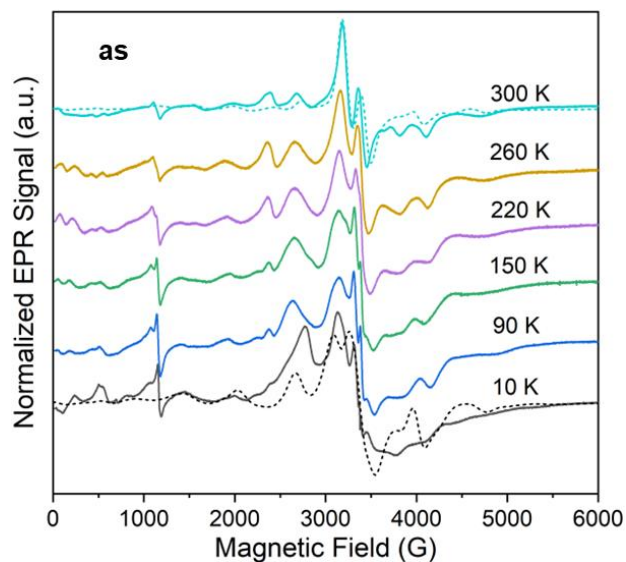


Figure S46. Variable-temperature CW EPR spectra of **La-Gd-LOF1_as**. The dashed lines represent the simulated spectra at 10 and 300 K.

References

- (1) Lin, Z.; Zou, R.; Liang, J. Xia, W.; Xia, D.; Wang, Y.; Lin, J.; Hu, T.; Chen, Q.; Wang, X.; Zhao, Y.; Burrell, A. K. Pore Size-Controlled Gases and Alcohols Separation within Ultramicroporous Homochiral Lanthanide-Organic Frameworks. *J. Mater. Chem.* **2012**, *22*, 7813–7818.
- (2) Sheldrick, G. M. SHELXT - Integrated Space-Group and Crystal-Structure Determination. *Acta Crystallogr. Sect. A Found. Crystallogr.* **2015**, *71*, 3–8.
- (3) Dolomanov, O. V.; Bourhis, L. J.; Gildea, R. J.; Howard, J. A. K.; Puschmann, H. OLEX2: A Complete Structure Solution, Refinement and Analysis Program. *J. Appl. Crystallogr.* **2009**, *42*, 339–341.
- (4) Sheldrick, G. M. Crystal Structure Refinement with SHELXL. *Acta Crystallogr. Sect. C Struct. Chem.* **2015**, *71*, 3–8.
- (5) Lin, Z.; Zou, R.; Xia, W.; Chen, L.; Wang, X.; Liao, F.; Wang, Y.; Lin, J.; Burrell, A. K. Ultrasensitive Sorption Behavior of Isostructural Lanthanide-Organic Frameworks Induced by Lanthanide Contraction. *J. Mater. Chem.* **2012**, *22*, 21076–21084.